ELSEVIER

Journal of Fluids and Structures 22 (2006) 997–1028

JOURNAL OF FLUIDS AND STRUCTURES

www.elsevier.com/locate/jfs

External shock loading on a submerged fluid-filled cylindrical shell

S. Iakovlev

Department of Engineering Mathematics, Dalhousie University, Halifax, Nova Scotia, Canada B3J 2X4

Received 21 December 2004; accepted 13 March 2006
Available online 23 August 2006

Abstract

The interaction between a submerged fluid-filled elastic circular cylindrical shell and an external shock wave is considered. The study focuses on the internal acoustic field. A linear formulation of the problem is considered. A semi-analytical solution is obtained and used to simulate the interaction. A variety of phenomena are observed in the internal fluid, including the reflection and focusing of the internal acoustic wave as well as the radiation into the fluid of elastic waves propagating in the shell. Throughout the paper, the results of numerical simulations are compared with available experimental data, and a good agreement is observed. The solution developed appears to be suitable for use as a benchmark. Engineering relevance of the phenomena observed is discussed.

1. Introduction

The interaction between shock waves and cylindrical shells has been extensively studied for the past five decades, and an enormous effort has been put into investigating various aspects of this complex multi-physics phenomenon. This is not surprising at all since circular cylindrical shells are one of the most commonly used construction members in a wide variety of engineering structures. Specifically, the offshore, naval, aerospace, nuclear, chemical and petroleum industries all extensively employ fluid-interacting cylindrical shell structures. Shock loads are a major threat to the safety of structures and installations common to the industries mentioned, and so the study of shock–shell interaction has always been of significant practical interest.

From the research point of view, study of the interaction between shock waves and shells is always challenging, both theoretically and experimentally. First of all, one has to deal with at least two, often more, coupled media which are reacting to a shock very differently. Furthermore, the interaction is a non-stationary and high-frequency process. Many complex phenomena, such as cavitation, interaction with detonation bubble, and water jet impact contribute to the interaction. Plastic deformations and structural failure often have to be considered as well. This complexity makes experiments involving shells and shock waves very technically demanding and costly, and the only alternative to those is mathematical modelling. The latter presents the researcher with many challenges as well, and adequate numerical simulation of shell–shock interaction remains a topic of active research interest to this day.

The first attempts to approach the interaction between circular cylindrical shells and shock waves date back to the early 1950s. At that time, the interest to the type of fluid–structure interaction in question was induced primarily by the

E-mail address: serguei.iakovlev@dal.ca.

0889-9746/$ - see front matter © 2006 Elsevier Ltd. All rights reserved.
doi:10.1016/j.jfluidstructs.2006.03.006

Nomenclature

c_f	sound speed in the fluid, $\hat{c}_f = 1$
c_s	sound speed in the shell material, $\hat{c}_s = c_s c_f^{-1}$
h_0	thickness of the shell, $\hat{h}_0 = h_0 r_0^{-1}$
I_n	modified Bessel function of the first kind of order n
K_n	modified Bessel function of the second kind of order n
p_α	peak incident pressure, $\hat{p}_\alpha = p_\alpha \rho_f^{-1} c_f^{-2}$
p_e	pressure in the external fluid, $\hat{p}_e = p_e \rho_f^{-1} c_f^{-2}$
p_i	pressure in the internal fluid, $\hat{p}_i = p_i \rho_f^{-1} c_f^{-2}$
p_0	incident pressure, $\hat{p}_0 = p_0 \rho_f^{-1} c_f^{-2}$
p_d	diffraction pressure, $\hat{p}_d = p_d \rho_f^{-1} c_f^{-2}$
p_r^e	external radiation pressure, $\hat{p}_r^e = p_r^e \rho_f^{-1} c_f^{-2}$
p_r^i	internal radiation pressure, $\hat{p}_r^i = p_r^i \rho_f^{-1} c_f^{-2}$
p_s	total pressure on the shell surface, $\hat{p}_s = p_s \rho_f^{-1} c_f^{-2}$
r	radial coordinate of the polar coordinate system, $r = \varrho r_0^{-1}$
r_0	radius of the shell, $\hat{r}_0 = 1$
R_0	radial distance to the source of the incident wave, $\hat{R}_0 = R_0 r_0^{-1}$
S_R	incident shock wave stand-off, $\hat{S}_R = S_R r_0^{-1}$
t	time, $t = \tau c_f r_0^{-1}$
v^*	transverse displacement of the middle surface of the shell, $v = v^* r_0^{-1}$
w^*	normal displacement of the middle surface of the shell, $w = w^* r_0^{-1}$
ε	strain in the middle surface of the shell, $\hat{\varepsilon} = \varepsilon$
θ	angular coordinate of the polar coordinate system
λ	exponential decay rate, $\hat{\lambda} = \lambda c_f r_0^{-1}$
ν	Poisson's ratio
ξ_n^i	'volume' response functions, internal fluid
ξ_n^e	'volume' response functions, external fluid
ρ_f	density of the fluid, $\rho_f = 1$
ρ_s	density of the shell material, $\hat{\rho}_s = \rho_s \rho_f^{-1}$
ϱ	radial coordinate of the polar coordinate system, $r = \varrho r_0^{-1}$
τ	time, $t = \tau c_f r_0^{-1}$
ϕ_e	fluid velocity potential in the external fluid, $\hat{\phi}_e = \phi_e c_f^{-1} r_0^{-1}$
ϕ_i	fluid velocity potential in the internal fluid, $\hat{\phi}_i = \phi_i c_f^{-1} r_0^{-1}$
ϕ_0	fluid velocity potential in the incident wave, $\hat{\phi}_0 = \phi_0 c_f^{-1} r_0^{-1}$
ϕ_d	fluid velocity potential in the diffracted wave, $\hat{\phi}_d = \phi_d c_f^{-1} r_0^{-1}$
ϕ_r^e	fluid velocity potential in the external radiated wave, $\hat{\phi}_r^e = \phi_r^e c_f^{-1} r_0^{-1}$
ϕ_r^i	fluid velocity potential in the internal radiated wave, $\hat{\phi}_r^i = \phi_r^i c_f^{-1} r_0^{-1}$
ψ_n^i	'surface' response functions, internal fluid
ψ_n^e	'surface' response functions, external fluid

$(*)_n \sin n\theta$ and $(*)_n \cos n\theta$ denote the harmonics of (*). Unless stated otherwise, capitalized symbols denote the Laplace transforms of the corresponding functions. Other symbols are defined in the text.

needs of the naval industry, and the research focus was on structural analysis. Mindlin and Bleich (1953) considered the early stages on the interaction between a plane shock wave and a circular cylindrical shell, and only analyzed dilatational and flexural modes. Haywood (1958) addressed the same plane wave impinging on a cylindrical shell but introduced a better early-time approximation. Peralta and Raynor (1964) considered the initial response of a fluid-filled cylindrical shell to an external shock wave and analyzed the shell velocity and diffraction pressure. Geers (1969) obtained an exact analytical solution of the problem of the interaction between a plane shock wave and a cylindrical shell using a combination of the modal expansion and the Laplace transform approach, and considered the total response of the shell.

Huang and Wang (1970) considered the interaction between a spherical shock wave and a circular cylindrical shell, and obtained an analytical solution using the Laplace–Fourier transform methodology combined with the modal approach. Stresses and strains were analyzed at a number of points, and comparison with the plane wave case was presented. An early-time solution of the same problem was obtained by Huang and Wang (1971), and the diffraction pressure was computed at several points on the shell surface. Geers (1972) considered scattering by a cylindrical shell of a plane acoustic wave and presented a detailed study of the diffraction pressure on the shell surface. Huang (1975) addressed scattering of a spherical shock wave by a rigid cylinder, and employed separation of variables and the Laplace transform. The surface pressure was discussed, and a formula linking the two- and three-dimensional solutions was introduced. Huang (1979) considered the response of a system of two co-axial cylindrical shells to a plane shock wave and analyzed the shell dynamics.

Even though we only mentioned some of the studies published, it appears that the vast majority of the researchers in the 1950–1970s were focusing on structural analysis, not the acoustic phenomena. The acoustic pressure induced during the interaction was often viewed as an 'external loading' which had to be determined to analyze stress–strain states. However, advanced analysis of engineering structures requires in-depth understanding of all the

aspects of the interaction. To that end, the acoustics of the interaction appears to be not less important than the structural analysis.

This, of course, was clearly understood a long time ago. Before it was possible to numerically simulate two- and three-dimensional shell–shock interaction, many experiments were conducted to visualize shock-induced pressure fields. For example, Bryson and Gross (1961) considered diffraction of strong shock waves by various solid bodies, in particular circular cylinders, and published several photographs of shock diffraction that were used for comparison by many researchers later on. Heilig (1969) considered diffraction of a shock wave by cylinders of various radii, and visualized the diffraction process using shadowgrams.

It appears, however, that shock-induced acoustic fields had not been a subject of extensive numerical study up until the mid 1980s when significant advances in computational technologies made numerical simulation of the interaction possible. For example, Yang et al. (1985) considered diffraction of strong plane shocks by various curved surfaces, in particular cylindrical. That study was extended to the case of a shock diffraction by a circular cylinder by Yang and Liu (1987) who presented detailed analysis of the acoustic fields. Glass et al. (1989) considered diffraction of a shock wave on a semi-circular cylinder and presented comparison to experimental results, and Eidelman et al. (1993) investigated shock wave diffraction by a cylinder in a dusty flow.

Experimental techniques were advancing as well, and many high-quality visualizations of shock–structure interaction appeared in the literature. We will only mention a few of them. Takayama (1987) considered shock wave propagation over a cylinder in a dusty gas flow, Heilig (1987) addressed various aspects of the shock wave reflection from a cylindrical surface, Hermann et al. (1987) studied vortex shedding from a cylinder in a shock flow, Sugiyama et al. (1989) considered a shock-induced flow past a circular cylinder in a dusty flow and presented some numerical results as well, and Takayama (1993) addressed a shock flow outside and inside a cylinder with a slotted surface.

Further development of numerical methods and computational technologies made possible a much more comprehensive analysis of the shell–shock interaction. In particular, it became possible to model many complex physical phenomena (e.g., cavitation, gas bubble formation and dynamics, viscosity effects, turbulence etc.). Incorporating those into modelling of the interaction brought the analysis of shock–shell interaction to a new level of sophistication.

For example, Ofengeim and Drikakis (1997) and Drikakis et al. (1997) numerically addressed diffraction of a plane shock wave by a rigid cylinder, and considered both inviscid and viscous models. Interaction at various Mach numbers was analyzed, and the effect of viscosity in various regions and at various times was discussed. Sun et al. (2003) investigated the interaction between a shock wave and a rotating cylinder both numerically and experimentally.

Takano et al. (1997) considered stresses in elastic cylinders subjected to an external shock wave, and also analyzed the surface-radiated acoustic waves. Sun (1998) studied shock wave diffraction on bodies of various shapes numerically, and compared numerical simulations to experimental results. Heilig (1999) studied shock wave propagation over a circular cylinder employing both numerical methods and experimental techniques and addressed a two-cylinder arrangement as well.

Oakley et al. (1999) considered the interaction of a shock wave with a hollow cylinder aiming at modelling impulsive shock loading on cooling tubes of an inertial confinement fusion reactor, and studied the interaction both experimentally and numerically. Pressure and acceleration time-histories were reported, and numerical simulations were compared to experimental shadowgrams. The study was extended (Oakley et al., 2001) to an arrangement of three cylinders, which was a much more realistic representation of the geometry of the reactor in question.

Wardlaw and Luton (2000) considered an explosion inside a fluid-filled cylindrical shell, focusing their study on the internal pressure fields and the dynamics of the shell. The interaction was simulated numerically, and a number of experiments were carried out. The influence of the shock–bubble interaction and the cavitation collapse on the interaction was investigated. Single- and double-walled cylinders were considered, and both rigid and deformable models were analyzed. Chambers et al. (2001) experimentally analyzed pressure on the inner surface of a water-filled aluminum shell subjected to an internal explosion, and presented comparison with numerical simulations. Sandusky et al. (1999) conducted a series of experiments to study the response of a fluid-filled shell to an internal explosion. Plastic deformations of the shell were analyzed, and the wall velocity and displacement, as well as strain, were measured. Preliminary numerical simulations were used to design the experiment.

Some work was devoted to shock wave focusing in reflectors of various shapes. Although these studies are not directly related to shell-structure interaction, they provide valuable reference information for analysis of internal acoustic fields. Sturtevant and Kulkarny (1976) experimentally studied focusing of shock waves in cylindrical reflectors. Sommerfeld and Muller (1988) presented experimental and numerical study of shock wave focusing by ellipsoidal and parabolic reflectors in water. Izumi et al. (1994) studied reflection and focusing of shock waves from parabolic reflectors. Schedin et al. (1997) experimentally investigated shock wave propagation and reflection in an elliptic cavity.

Sun and Takayama (1996) conducted experiments to analyze focusing in a circular reflector, and such focusing was further addressed numerically by Sun (1998) and Sun and Takayama (1999). Liang et al. (1999) studied focusing of shock waves in parabolic reflectors, and presented visualization of numerical results as well as some comparison to experiments. Apazidis (2003) numerically addressed focusing of shock waves in an elliptic cavity, and established some interesting features of focusing in elliptic reflectors.

As to more complex systems involving cylindrical structures, we will mention studies of Yang et al. (1991) who presented numerical simulations of shock wave diffraction on an elliptic cylinder at different angles of attack, Jialing and Hongli (1997) who addressed numerically and experimentally shock wave propagation over a two-cylinder arrangement, Abe et al. (1999) who considered shock wave propagation over an array of circular cylinders, and Lind et al. (1999) who investigated shock wave attenuation by a structure consisting of two perpendicular arrays of cylindrical rods. Andelfinger (1994) considered an underwater explosion against a cylindrical shell with end closures and external stiffeners, and numerically analyzed external pressure field and plastic deformations of the structure; comparison to experimental results was presented as well.

This literature review would not be complete without mentioning the considerable computational and experimental effort that has been put into studying shock interaction with structures of complex geometry. Of those, the most challenging is modelling of real-life industrial structures, for example ships [e.g., Aanhold et al. (1998), Shin and Santiago (1998), Park et al. (2003)]. Extensive reviews of the literature pertaining to analysis of the response of submerged structures to underwater explosions can be found, for example, in the compilations by Mair (1999b) where analytical, numerical, and experimental studies are discussed, and Mair (1999a) which focuses on numerical approaches.

Even though the recent research effort seems to have been focused on numerical modelling of shell–shock interaction, analytical and hybrid analytical–numerical solutions are still being successfully employed. For example, doubly asymptotic approximations have been proven as an extremely efficient technique of fluid–structure interaction analysis [e.g., Geers and Zhang (1994a, b)]. Furthermore, converged analytical solutions are extensively used as benchmarks for verification of numerical codes (Mair, 1999b), therefore some attention is still being paid to analytical approaches [e.g., Huang and Mair (1996), Sprague and Geers (1999)]. As to semi-analytical approaches, Iakovlev (2002a) studied stress–strain state of a fluid-filled submerged cylindrical shell subjected to a spherical shock wave, and Iakovlev (2004) considered the dynamics of such a system incorporating a rigid coaxial cylindrical core. Another example of a semi-analytical approach is the study of Liang et al. (2000) who coupled the finite element method with the doubly asymptotic approximations to investigate the response of a submerged spherical shell to an external shock wave.

As this analysis of the literature indicates, it appears that the *internal* acoustic field induced by an *external* shock wave in a submerged fluid-filled circular cylindrical shell has not yet been addressed. Study of this aspect of shock–shell interaction is the main objective of this paper.

Furthermore, if an acceptable agreement between available experimental data and the numerical simulations based on the solution obtained here is established, the latter will be suitable for use as a benchmark. It appears that such a benchmark would be a useful addition to the existing set of converged analytical solutions used by the underwater explosion community (Mair, 1999b). Also, if the proposed methodology turns out to be successful for rather a simple system considered here, it will be possible to confidently use it for analysis of much more complex shell systems. Thus, another goal of the present study is to build a foundation for future research, including a variety of visualization techniques and computer codes facilitating fluid–structure interaction analysis of shock-subjected shells. In view of that, special attention is paid throughout the paper to experimental verification of the results obtained.

Discussing benchmark solutions, we would like to particularly emphasize that most of the benchmarks currently in use are those providing information about structural dynamics, not acoustic fields. Thus, it would be of practical value to produce benchmarks that would allow for simulation of pressure fields for several common geometries and be therefore suitable for verification of both structural analysis codes *and* the codes aimed at analysis of acoustic fields induced during shell–shock interaction. In this light, the present work is first in a series of semi-analytical studies the author intends to publish.

Finally, we mention that there is one more reason for considering the internal acoustic field induced by an external shock wave. As it has been shown in the author's earlier studies [e.g., Iakovlev (2002a) and particularly Iakovlev (2004)], many important elastic effects in the shell are due to acoustic phenomena in the internal fluid. Even though there was no doubt about the connection between the dynamics of the stress–strain state and the acoustics of the internal fluid, the analysis carried out was 'implicit', i.e. the internal pressure field itself was not analyzed, and the conclusions drawn were based on what was observed on the surface of the shell. Thus, it would definitely be of interest to study the internal field directly, and to actually visualize the acoustic waves that were seen to cause significant changes in the stress–strain state.

2. Mathematical formulation

We consider a circular cylindrical shell of radius r_0 and thickness h_0. We assume that $h_0/r_0 \ll 1$, and also that the deflections of the shell surface are small comparatively to its thickness, so linear theory of shells is applicable. The transverse and normal middle surface displacements are v^* and w^*, respectively. The shell material is characterized by density ρ_s, sound speed c_s and Poisson's ratio ν. The shell is submerged into and filled with linearly compressible, irrotational, non-viscous fluid of density ρ_f. The sound speed in the fluid is c_f. We assume that the shell is subjected to a cylindrical shock wave whose source is located at the distance R_0 from the axis of the shell. Polar coordinates (ϱ, θ) based on the axis of the shell are employed. The schematic of the problem is shown in Fig. 1.

The assumption of a cylindrical incident wave implies a two-dimensional simplification of the generally three-dimensional problem. Analysis indicated that, while enormously reducing computational time, such a simplified model captures the most important dynamic features of the interaction really well. Note also that we consider the simplest two-fluid model, i.e. we assume that the same fluid is both inside and outside the shell. This allows us to concentrate on the most important dynamic features of the shell–fluid interaction without bringing in the complexity of a system consisting of three different media. We note that, even though the solution for the general case of two different fluids would be just slightly more complex, preliminary analysis shows that the resulting acoustic fields would be qualitatively different. Addressing the general case of two different fluids is one of the author's future research objectives.

The fluids are governed by the wave equations

$$\nabla^2\phi_e = \frac{1}{c_f^2}\frac{\partial^2\phi_e}{\partial\tau^2} \quad \text{and} \quad \nabla^2\phi_i = \frac{1}{c_f^2}\frac{\partial^2\phi_i}{\partial\tau^2}, \tag{1}$$

where ϕ_e and ϕ_i are the fluid velocity potentials in the external and internal fluids, respectively, and τ is time.

The shell equations in displacements are [the equations assume the Love–Kirchhoff hypothesis, and their detailed derivation can be found, for example, in Junger and Feit (1972)]

$$\frac{1}{r_0^2}\frac{\partial^2 v^*}{\partial\theta^2} - \frac{1}{r_0^2}\frac{\partial w^*}{\partial\theta} + k_0^2\left(\frac{1}{r_0^2}\frac{\partial^3 w^*}{\partial\theta^3} + \frac{1}{r_0^2}\frac{\partial^2 v^*}{\partial\theta^2}\right) = \frac{1}{c_s^2}\frac{\partial^2 v^*}{\partial\tau^2}, \tag{2}$$

$$\frac{1}{r_0^2}w^* - \frac{1}{r_0^2}\frac{\partial v^*}{\partial\theta} + k_0^2\left(\frac{1}{r_0^2}\frac{\partial^4 w^*}{\partial\theta^4} + \frac{1}{r_0^2}\frac{\partial^3 v^*}{\partial\theta^3}\right) = \chi p_s - \frac{1}{c_s^2}\frac{\partial^2 w^*}{\partial\tau^2}, \tag{3}$$

where $k_0^2 = h_0^2/(12r_0^2)$, $\chi = (h_0\rho_s c_s^2)^{-1}$, and p_s is the pressure acting upon the shell surface. The strain in the middle surface of the shell is given by

$$\varepsilon = \frac{1}{r_0}\left(\frac{\partial v^*}{\partial\theta} - w^*\right). \tag{4}$$

We note that in many practical situations, some terms in (2) and (3) can be neglected without changing the resulting displacements significantly [e.g., Ugural (1981), Scott (1988)]. We, however, consider the most complete version given by Eqs. (2) and (3).

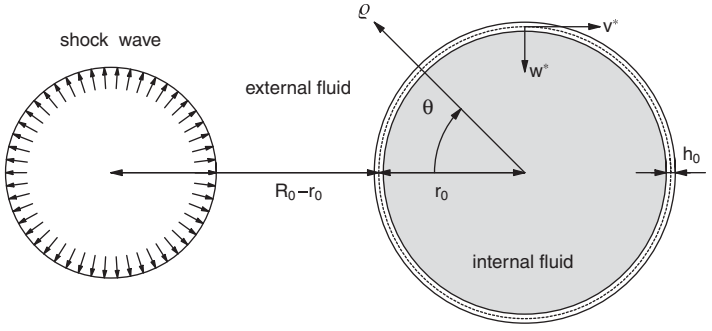

Fig. 1. Schematic of the problem.

The external pressure, p_e, is contributed by the incident pressure p_0, diffraction pressure p_d, and external radiation pressure p_r^e,

$$p_e = p_0 + p_d + p_r^e, \tag{5}$$

whereas the internal acoustic field is completely determined by the internal radiation pressure, $p_i = p_r^i$. The total pressure p_s acting upon the shell is

$$p_s = (p_0 + p_d + p_r^e - p_r^i)|_{\varrho=r_0}. \tag{6}$$

The total fluid velocity potentials ϕ_e and ϕ_i are

$$\phi_e = \phi_0 + \phi_d + \phi_r^e \tag{7}$$

and

$$\phi_i = \phi_r^i, \tag{8}$$

where ϕ_0, ϕ_d, ϕ_r^e, and ϕ_r^i are the potentials in the incident shock wave, diffracted wave, external radiated wave, and internal radiated wave, respectively. The equations for p_0 and ϕ_0, along with their derivation, can be found in Appendix B.

The boundary conditions on the shell surface are

$$\left.\frac{\partial\phi_r^e}{\partial\varrho}\right|_{\varrho=r_0} = -\frac{\partial w^*}{\partial\tau}, \tag{9}$$

$$\left.\frac{\partial\phi_r^i}{\partial\varrho}\right|_{\varrho=r_0} = -\frac{\partial w^*}{\partial\tau}, \tag{10}$$

and

$$\left.\frac{\partial\phi_d}{\partial\varrho}\right|_{\varrho=r_0} = -\left.\frac{\partial\phi_0}{\partial\varrho}\right|_{\varrho=r_0}, \tag{11}$$

along with the conditions at the infinity,

$$\phi_d \longrightarrow 0 \quad \text{and} \quad \phi_r^e \longrightarrow 0 \quad \text{when} \quad \varrho \to \infty. \tag{12}$$

We also require the internal potential to be bounded on the axis of the shell, and assume appropriate periodicity conditions θ-wise as well as zero initial conditions.

To make the results applicable to a wider range of practical situations, and to avoid dealing with small numerical values of τ, we introduce a dimensionless formulation of the problem, and normalize all variables to r_0, c_f, and ρ_f. With some exceptions (namely, the shell surface displacements, time, and radial coordinate), a hat over a dimensionless variable is used to distinguish it from its dimensional counterpart. From here on, we mostly consider dimensionless variables. However, acoustic fields are analyzed in dimensional form, which seems to be more appropriate for practice-oriented analysis.

Before we proceed to the discussion of the solution, we outline the dimensionless formulation of the problem. The dimensionless wave equations are

$$\nabla^2\hat{\phi}_e = \frac{\partial^2\hat{\phi}_e}{\partial t^2} \quad \text{and} \quad \nabla^2\hat{\phi}_i = \frac{\partial^2\hat{\phi}_i}{\partial t^2}, \tag{13}$$

and the equations of shell dynamics are

$$\frac{\partial^2 v}{\partial\theta^2} - \frac{\partial w}{\partial\theta} + k_0^2\left(\frac{\partial^3 w}{\partial\theta^3} + \frac{\partial^2 v}{\partial\theta^2}\right) = \frac{1}{\hat{c}_s^2}\frac{\partial^2 v}{\partial t^2}, \tag{14}$$

$$w - \frac{\partial v}{\partial\theta} + k_0^2\left(\frac{\partial^4 w}{\partial\theta^4} + \frac{\partial^3 v}{\partial\theta^3}\right) = \hat{\chi}\hat{p}_s - \frac{1}{\hat{c}_s^2}\frac{\partial^2 w}{\partial t^2}, \tag{15}$$

where $\hat{\chi} = (\hat{\rho}_s\hat{c}_s^2\hat{h}_0)^{-1}$. The strain expressed in terms of the dimensionless displacements is

$$\varepsilon = \frac{\partial v}{\partial\theta} - w. \tag{16}$$

The dimensionless boundary conditions are

$$\left.\frac{\partial\hat{\phi}_r^e}{\partial r}\right|_{r=1} = -\frac{\partial w}{\partial t}, \tag{17}$$

$$\left.\frac{\partial\hat{\phi}_r^i}{\partial r}\right|_{r=1} = -\frac{\partial w}{\partial t}, \tag{18}$$

and

$$\left.\frac{\partial\hat{\phi}_d}{\partial r}\right|_{r=1} = -\left.\frac{\partial\hat{\phi}_0}{\partial r}\right|_{r=1}, \tag{19}$$

along with the conditions at the infinity,

$$\hat{\phi}_d \longrightarrow 0 \quad \text{and} \quad \hat{\phi}_r^e \longrightarrow 0 \quad \text{when} \quad r \to \infty. \tag{20}$$

3. Acoustics

The approach we use to treat the acoustic part of the problem is rather standard. We apply the Laplace transform time-wise to the dimensionless wave equations (13) to obtain

$$\frac{\partial^2\hat{\Phi}_e}{\partial r^2} + \frac{1}{r}\frac{\partial\hat{\Phi}_e}{\partial r} + \frac{1}{r^2}\frac{\partial^2\hat{\Phi}_e}{\partial\theta^2} - s^2\hat{\Phi}_e = 0, \tag{21}$$

and

$$\frac{\partial^2\hat{\Phi}_i}{\partial r^2} + \frac{1}{r}\frac{\partial\hat{\Phi}_i}{\partial r} + \frac{1}{r^2}\frac{\partial^2\hat{\Phi}_i}{\partial\theta^2} - s^2\hat{\Phi}_i = 0, \tag{22}$$

where $\hat{\Phi}_e$ and $\hat{\Phi}_i$ are the Laplace transforms of $\hat{\phi}_e$ and $\hat{\phi}_i$, respectively, and s is the transform variable. Then we use separation of variables θ-wise which yields the general solution of (21) and (22) in the form

$$\hat{\Phi} = \{F_n \mathrm{I}_n(rs) + G_n \mathrm{K}_n(rs)\}\cos n\theta, \quad n = 0, 1, \ldots, \tag{23}$$

where I_n and K_n are the modified Bessel functions of order n of the first and second kind, respectively, and F_n and G_n are arbitrary functions of s. After the boundary conditions are imposed, the Laplace transforms of the harmonics of the three unknown potential components are obtained:

$$\hat{\Phi}_n^d = B_n \Xi_n^e \cos n\theta, \tag{24}$$

$$\hat{\Phi}_n^{r,e} = sW_n \Xi_n^e \cos n\theta, \tag{25}$$

and

$$\hat{\Phi}_n^{r,i} = -sW_n \Xi_n^i \cos n\theta. \tag{26}$$

Here B_n and W_n are the Laplace transforms of b_n and w_n, respectively, where

$$\left.\frac{\partial\hat{\phi}_0}{\partial r}\right|_{r=1} = \sum_{n=0}^{\infty} b_n(t)\cos n\theta, \tag{27}$$

and

$$w = \sum_{n=0}^{\infty} w_n(t)\cos n\theta, \tag{28}$$

and $\xi_n^e(r,t)$ and $\xi_n^i(r,t)$ are the 'response functions' of the problem, the Laplace transforms of which, $\Xi_n^e(r,s)$ and $\Xi_n^i(r,s)$, respectively, are given by

$$\Xi_n^e(r,s) = -\frac{\mathrm{K}_n(rs)}{s\mathrm{K}_n'(s)}, \tag{29}$$

and

$$\Xi_n^i(r,s) = \frac{\mathrm{I}_n(rs)}{s\mathrm{I}_n'(s)}. \tag{30}$$

The functions $\xi_n^e(r,t)$ and $\xi_n^i(r,t)$ represent the response of the external and internal fluids, respectively, to the motion of and scattering by the shell, and are discussed later. It is important to point out that the response functions we consider here represent pressure not only on the shell surface, but *anywhere* in the fluids; and so they can be referred to as the 'volume' response functions, as opposed to the 'surface' response functions that appear when the pressure is only studied on the shell surface. Setting $r = 1$ reduces the 'volume' response functions $\xi_n^e(r,t)$ and $\xi_n^i(r,t)$ to their 'surface' counterparts $\psi_n^e(t)$ and $\psi_n^i(t)$, respectively (Iakovlev, 2002a, 2004), the Laplace transforms of which are

$$\Psi_n^e(s) = -\frac{\mathrm{K}_n(s)}{s\mathrm{K}_n'(s)}, \tag{31}$$

and

$$\Psi_n^i(s) = \frac{\mathrm{I}_n(s)}{s\mathrm{I}_n'(s)}. \tag{32}$$

Since our main objective is the internal acoustic field, the external pressure is only considered on the outer surface of the shell. Applying some theorems related to the Laplace transform to (24) and (25), the two unknown components of the external pressure on the shell surface can be obtained as

$$\hat{p}_d|_{r=1} = \sum_{n=0}^{\infty} \hat{p}_n^d(t)\cos n\theta, \tag{33}$$

and

$$\hat{p}_r^e|_{r=1} = \sum_{n=0}^{\infty} \hat{p}_n^{r,e}(t)\cos n\theta, \tag{34}$$

where

$$\hat{p}_n^d = -b_n(t) - \int_0^t b_n(\eta)\frac{\mathrm{d}\psi_n^e}{\mathrm{d}\eta}(t-\eta)\,\mathrm{d}\eta, \tag{35}$$

and

$$\hat{p}_n^{r,e} = -\int_0^t \frac{\mathrm{d}^2 w_n(\eta)}{\mathrm{d}\eta^2}\psi_n^e(t-\eta)\,\mathrm{d}\eta. \tag{36}$$

Eqs. (33) and (34), along with the modal representation of the incident pressure on the shell surface,

$$\hat{p}_0|_{r=1} = \sum_{n=0}^{\infty} \hat{p}_n^0(t)\cos n\theta, \tag{37}$$

completely determine the total pressure on the outer surface of the shell.

The internal pressure is easily obtained as

$$\hat{p}_r^i = \sum_{n=0}^{\infty} \hat{p}_n^{r,i}(r,t)\cos n\theta, \tag{38}$$

where

$$\hat{p}_n^{r,i} = \int_0^t \frac{\mathrm{d}^2 w_n(\eta)}{\mathrm{d}\eta^2}\,\xi_n^i(r,t-\eta)\,\mathrm{d}\eta. \tag{39}$$

Note that, unlike (33)–(36), Eqs. (38) and (39) allow for computation of the pressure *anywhere* inside the shell.

Note also that setting $r = 1$ reduces (38) to the equation for the internal pressure on the inner shell surface,

$$\hat{p}_r^i|_{r=1} = \sum_{n=0}^{\infty} \hat{p}_n^{r,i}|_{r=1}\cos n\theta, \tag{40}$$

where

$$\hat{p}_n^{r,i}|_{r=1} = \int_0^t \frac{\mathrm{d}^2 w_n(\eta)}{\mathrm{d}\eta^2} \xi_n^i(r, t-\eta)|_{r=1}\,\mathrm{d}\eta \tag{41}$$

$$= \int_0^t \frac{\mathrm{d}^2 w_n(\eta)}{\mathrm{d}\eta^2} \psi_n^i(t-\eta)\,\mathrm{d}\eta. \tag{42}$$

The total acoustic load on the shell surface can therefore be written as

$$\hat{p}_s = \sum_{n=0}^{\infty} \hat{p}_n^s(t) \cos n\theta, \tag{43}$$

where

$$\hat{p}_n^s = \hat{p}_n^0 + \hat{p}_n^d + \hat{p}_n^{r,e} - \hat{p}_n^{r,i}|_{r=1}. \tag{44}$$

Thus, simulating the internal acoustic field is a two-step process. First, Eq. (43) is coupled with the shell equations to determine the normal displacements w. Second, the normal displacement is used to simulate the entire internal field using Eqs. (38) and (39).

We would like to emphasize that the first and second parts of the solution do not necessarily have to be approached with the same methodology. In fact, the normal displacements can be determined completely independently, and used later in Eqs. (38) and (39) to simulate the internal field. This seems to be an advantage of the solution proposed, since it allows one to simulate the internal field in *any* fluid-filled shell for which there is available a time-history of w over the entire cross-section of the shell. In particular, nothing appears to be stopping one from using experimental measurements of w in a real shell system, as long as none of the assumptions made are violated. This appears to be a promising direction for future research, since measurements of the normal displacement are much less technically challenging than those of the pressure anywhere inside the shell.

In order to solve the shell equations, one has to determine the unknown surface pressure components in (44). Those are expressed in terms of the convolution integrals which include the 'surface' response functions. The external ones, ψ_n^e, were introduced by Geers (1969) in a slightly different form, and their graphs along with a brief discussion can be found in Iakovlev (2004). The internal response functions ψ_n^i are analyzed in Iakovlev (2002b). Thus, all the information one needs to determine the displacements of the shell is readily available.

The situation with the second part of the solution is much more complicated. The convolution integral (39) includes the 'volume' internal response functions ξ_n^i which, to the best of the author's knowledge, have not been addressed yet. As it turned out, even though the analytical procedure developed for the 'surface' internal response functions ψ_n^i can be successfully applied to obtain analytical expressions for ξ_n^i, actual computation of ξ_n^i is challenging, as is their numerical integration. The analytical inversion of the Laplace transforms of ξ_n^i along with the discussion of a variety of issues associated with these functions can be found in Appendix A. Here we just mention that the behaviour of the 'volume' internal response functions is incomparably more complex than that of their surface counterparts, and a number of rather sophisticated algorithms had to be developed to deal with the associated numerical challenges. Note that in this work we do not consider the 'volume' external response functions ξ_n^e.

4. Shell dynamics

We expand the middle surface displacements v and w into the series

$$v = \sum_{n=0}^{\infty} v_n \sin n\theta \tag{45}$$

and

$$w = \sum_{n=0}^{\infty} w_n \cos n\theta, \tag{46}$$

and substitute the harmonics $v_n \sin n\theta$ and $w_n \cos n\theta$ into (2) and (3). This yields an integro-differential system for every n,

$$\gamma^2 \frac{\mathrm{d}^2 v_n}{\mathrm{d}t^2} + c_n^{11} v_n + c_n^{12} w_n = 0,$$

$$\gamma^2 \frac{\mathrm{d}^2 w_n}{\mathrm{d}t^2} + c_n^{21} v_n + c_n^{22} w_n = \hat{\chi} \hat{p}_n^s, \tag{47}$$

where

$$c_n^{11} = n^2 + k_0^2 n^2, \quad c_n^{12} = c_n^{21} = -n - k_0^2 n^3, \quad c_{mn}^{22} = 1 + k_0^2 n^4 \text{ and } \gamma = \hat{c}_s^{-1}, \tag{48}$$

all initial conditions are zero, and the total pressure on the shell surface $\hat{p}_n^s$ is given by (43). System (47) was approached numerically (finite differences).

Note that, in Eqs. (47), terms multiplied by $\hat{k}_0^2$ represent bending stiffness, so neglecting those terms would imply switching to a membrane model of deformation (from here on we shall refer to these terms as the 'bending terms'). The importance of taking the bending terms into account is often not apparent *a priori*, and comparison of the results produced by two models, with and without bending stiffness, for a specific load and a certain range of shell parameters is needed. Such analysis was carried out, and it was established that for a shell with the thickness-to-radius ratio of less than 0.01 the influence of the bending terms on the internal acoustic field is not significant, and is limited to a very high-frequency, low-magnitude contribution. Since shells with $h_0/r_0 \leqslant 0.01$ represent an important class of fluid-interacting thin-walled engineering structures, we shall focus our study on such shells, and shall assume from here on that bending stiffness can be neglected.

We also mention that, even though a semi-analytical approach was chosen in the present work, i.e. an analytical solution of the acoustic equations was coupled with a finite difference solution of the shell equations, it is possible to obtain a fully analytical solution of the problem. In that case, instead of applying a finite difference algorithm to system (47), the Laplace transform technique is used. The resulting system will be that of two algebraic equations for the transforms of v_n and w_n, and its solution will involve rather complex fractional expressions of semi-polynomial type in s with modified Bessel functions as the coefficients. Analytical inversion of such expressions is possible, but is hardly attractive from the practical point of view. Thus, one is left with only one option, i.e. numerical inversion.

In comparison with the finite-difference approach, that involving numerical inversion of the Laplace transform is much more time consuming. Furthermore, changing even one parameter of the shell will lead to a different set of Laplace transforms, and so the inversion will have to be repeated all over again. In contrast, when the finite difference approach is used and a number of different shells are considered, the components of the surface loading either do not change at all (incident and diffraction pressure) or are expressed in terms of the shell displacements and the response functions that are pre-computed (radiation pressure). Thus, changing the parameters of the shell only affects the final part of the solution, i.e. numerical coupling between the 'acoustic' and 'elastic' parts, which takes only a small fraction of the total computational time. Therefore, the semi-analytical approach proposed is not only more time-efficient, it is also more suitable when many shells with various parameters have to be analyzed.

For the sake of completeness, we applied the fully analytical Laplace transform approach to the 'test' case of a plane shock wave and a steel shell submerged into and filled with water, and compared the results versus the ones produced by the semi-analytical approach. An excellent agreement was observed, even though the computational time necessary to achieve similar accuracy was incomparable (in favour of the semi-analytical methodology).

5. Results and discussion

5.1. General discussion and terminology

We consider a steel shell with $\rho_s = 7800\ \mathrm{kg/m^3}$, $c_s = 5000\,\mathrm{m/s}$, and $h_0/r_0 = 0.01$ ($r_0 = 1\,\mathrm{m}$ and $h_0 = 0.01\,\mathrm{m}$). The shell is submerged into and filled with water, $\rho_f = 1000\ \mathrm{kg/m^3}$ and $c_f = 1400\,\mathrm{m/s}$.

In the shock wave diffraction theory, the term 'stagnation point' is used for the points $\theta = 0$ and $\theta = \pi$, with the point $\theta = 0$ being referred to as the 'front stagnation point', and the point $\theta = \pi$ being the 'rear stagnation point'. Although this terminology is perfectly appropriate for the case of a rigid cylinder, in the present case it does not seem to be a natural choice since the shell surface is moving. We suggest referring to these points as the 'head point' and 'tail point', respectively. We also suggest referring to the proximities of the head and tail points as the 'head region' and 'tail region', respectively.

At the very beginning of the interaction, the incident wave causes the shell surface in the head region to move. This motion results in an acoustic wave being originated in the internal fluid. The propagation, reflection, and interaction of this wave with the shell results in a variety of phenomena occurring in the system. Because of its importance, special terminology seems to be appropriate, and we suggest referring to this pressure wave as the 'internal shock wave'. This terminology is not exactly correct since the internal pressure wave is not a 'shock wave' in the classical sense. Namely, it does not have a front as such, i.e. there is no pressure discontinuity associated with it. However, as we shall see shortly, the corresponding pressure rise is very sharp, and so the proposed terminology seems to be acceptable.

To facilitate the study of the interaction, we divide it into three stages. Namely, we suggest calling the initial stage the 'downstream propagation'. The corresponding times are $t = 0.00 - 2.00$, i.e. from the instant when the incident shock wave impinges on the shell to the instant when the internal shock wave reaches the tail point. The mid-interaction is suggested to be referred to as the 'primary reflection and focusing'. The corresponding times are $t = 2.00 - 3.00$, i.e. from the instant the internal shock wave reflects from the tail region to the instant shortly after it focuses. Finally, we suggest using the term 'upstream propagation and secondary reflection and focusing' for the late interaction, $t = 3.00 - 5.00$, i.e. when the reflected wave propagates upstream, reflects from the head region and focuses again. Each of these stages has unique dynamic features and is considered separately.

As to the incident shock wave, we consider two distinctly different loadings. The first one is a large-stand-off shock wave (i.e. a shock wave with the source located at a significant distance from the shell, $\hat{R}_0 \gg 1$), and the second one is a small-stand-off shock wave (explosion occurs in the close proximity of the shell, $\hat{R}_0 \approx 1$). In the first case we set $\hat{R}_0 = 5.0$, and in the second one we assume $\hat{R}_0 = 1.1$. From the practical point of view, these waves represent two completely different interaction scenarios.

For a large-stand-off explosion, a single high-pressure front propagates in the external fluid and suddenly impinges on the shell. From the mathematical point of view, this is exactly what the linear model assumes. Thus, the results obtained for a large-stand-off case using the model employed here are expected to be quite close to what one would observe in a real system, and so analysis of such a loading is of particular practical importance.

In contrast, a small-stand-off shock wave is considered strictly for the purposes of comparison with available experimental data. The results produced by a linear model in the case of a close explosion hardly have any practical value: the interaction is dominated by strictly nonlinear phenomena such as detonation bubble expansion and collapse, water jet impact, and cavitation [e.g., Wardlaw and Luton (2000), Mair (1999b)]. Obviously, such interaction calls for a much more sophisticated model than the one considered here. However, it turns out that a very small-stand-off shock wave ($\hat{R}_0 = 1.1$) produces the internal shock wave of the exact same geometry as that considered in the experimental study we refer to later to verify our numerical results.

To estimate the parameters of a shock wave λ and p_α, one would normally use well-known empirical formulas [e.g., Cole (1948)]. For our purposes we assume $p_\alpha = 250\,\text{kPa}$ and $\lambda = 0.0001314\,\text{s}$ for both waves.

5.2. Downstream propagation

The internal pressure is induced by the motion of the shell surface, and evaluation of the integrals (39) is needed to simulate it. At the very beginning of the interaction, however, pressure is mostly determined by the normal velocity of the shell surface $\partial w/\partial t$. This can easily be shown mathematically if one recalls that $\psi_n^i(t) = 1 + O(t)$ when $t \ll 1$, and so

$$\hat{p}_n^{r,i} \approx \frac{\mathrm{d}w_n}{\mathrm{d}t}, \quad t \ll 1, \tag{49}$$

which implies

$$\hat{p}_r^i \approx \frac{\partial w}{\partial t}, \quad t \ll 1. \tag{50}$$

As a matter of fact, it can be shown that at the head point Eq. (50) works very well for $t \in [0, 0.5]$ for the large-stand-off incident wave considered. Eq. (50) is very helpful in understanding of how the internal shock wave is originated.

Fig. 2 shows the normal velocity of the shell surface in the beginning of the interaction. The velocity profiles were scaled so that the peak velocity is equal to 35% of the shell radius. The velocity reaches its maximum by $t \approx 0.07$ and, as a result, the pressure in the internal fluid changes from zero to its maximum over a very short period of time. This sudden pressure change induces a wave that we refer to as the 'internal shock wave'. It is clear now that even though this wave has no discontinuity associated with it, the pressure rise is almost vertical relative to the time it takes for the incident wave to move over the shell, and so it is quite reasonable to call it a 'shock wave'. We also note that the early interaction ($t = 0.00 - 0.25$) appears to be most critical for the formation of the internal shock wave, and almost completely determines the wave's shape and energy.

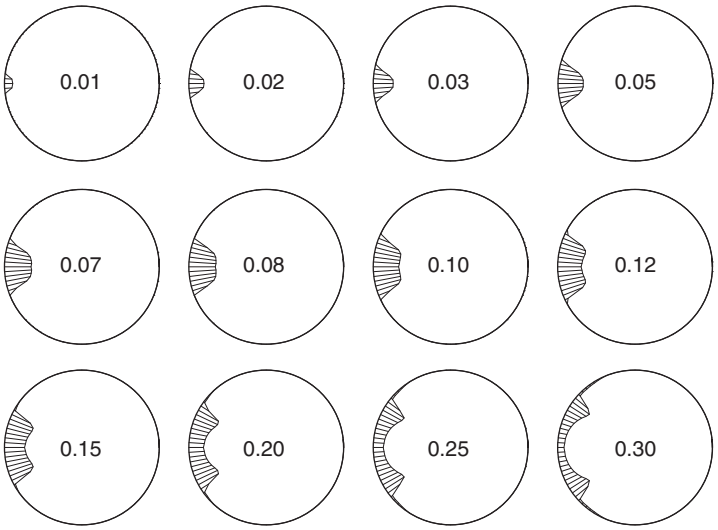

Fig. 2. Dynamics of the normal velocity of the shell surface at the beginning of the interaction.

Having understood how the internal shock wave is originated, we turn to the analysis of the most interesting aspect of the interaction, i.e. the dynamics of the internal pressure. Figs. 3 and 4 show a series of two-dimensional 'snapshots' of the internal acoustic field. Two different types of waves can be clearly identified. The first one is the internal shock wave itself, propagating at the velocity which is equal to that of sound in the internal fluid, and the second one being low-amplitude 'head' waves propagating in the proximity of the shell surface at a supersonic (relative to the fluid) velocity. These waves represent two qualitatively different phenomena occurring in the shell-fluid system, and are discussed separately.

5.2.1. Internal shock wave

We start with the analysis of the internal shock wave. Originated at the beginning of the interaction, it propagates through the internal fluid and reflects from the tail region at $t \approx 2$. The corresponding pressure patterns are quite regular, and resemble those of a shock wave originated at a point source. However, one can observe two formations that start to develop near the shell surface at $t > 1$, and whose presence becomes particularly apparent at $t > 1.5$. Pressure in the affected zones is considerably higher than that in the internal shock wave itself. Thus, even though local, these near-wall formations are important contributors to the interaction. Theoretically, there are two possible reasons for these formations to exist. First, it is possible that they are caused by an elastic phenomenon of some sort in the shell, and simply represent its radiation into the fluid. Another possibility is that these formations are a purely acoustic phenomenon, and are not linked to the elasticity of the shell.

To shed some light on the origins of these near-wall formations, we turn to related experimental results. In the absence of experimental data for shock wave reflection and focusing in fluid-filled elastic shells, we refer to the study by Sun and Takayama (1996) who investigated focusing of a shock wave in a circular reflector, and presented a number of high-resolution interferograms. We compare their experimental results for a weak shock wave (the Mach number of 1.1), Fig. 5(a) and (c), to the pressure patterns simulated numerically for the same instants, Fig. 5(b) and (d). As was discussed above, the small-stand-off shock wave is used in simulations. Note that in the experiments considered shock waves were generated in a shock tube that was connected to the circular reflector, and the vortex patterns observed are due to emerging of the shock wave from the nozzle of the driven channel. We ignore these irregularities and only focus on the wavefront region. Note also that the interferogram (a) shows two consecutive instants, and we only consider the later one. Slight blurriness in some parts of the simulated images is due to the fact that the internal pressure wave does not have a front, unlike a 'real' shock wave addressed in the experiments.

One can see that there is a good overall agreement between the experiments and numerical simulations. In particular, the near-wall formations in question are present in both cases, and very similar geometries of those are observed. Since the reflector in the experiments had solid walls, we can confidently conclude that the numerically observed near-wall formations are an acoustic phenomenon, and are not induced by elastic effects in the shell. As to the physics of these formations, they represent patterns inherent to regular reflection, as opposed to Mach reflection [e.g., Ben-Dor (1991),

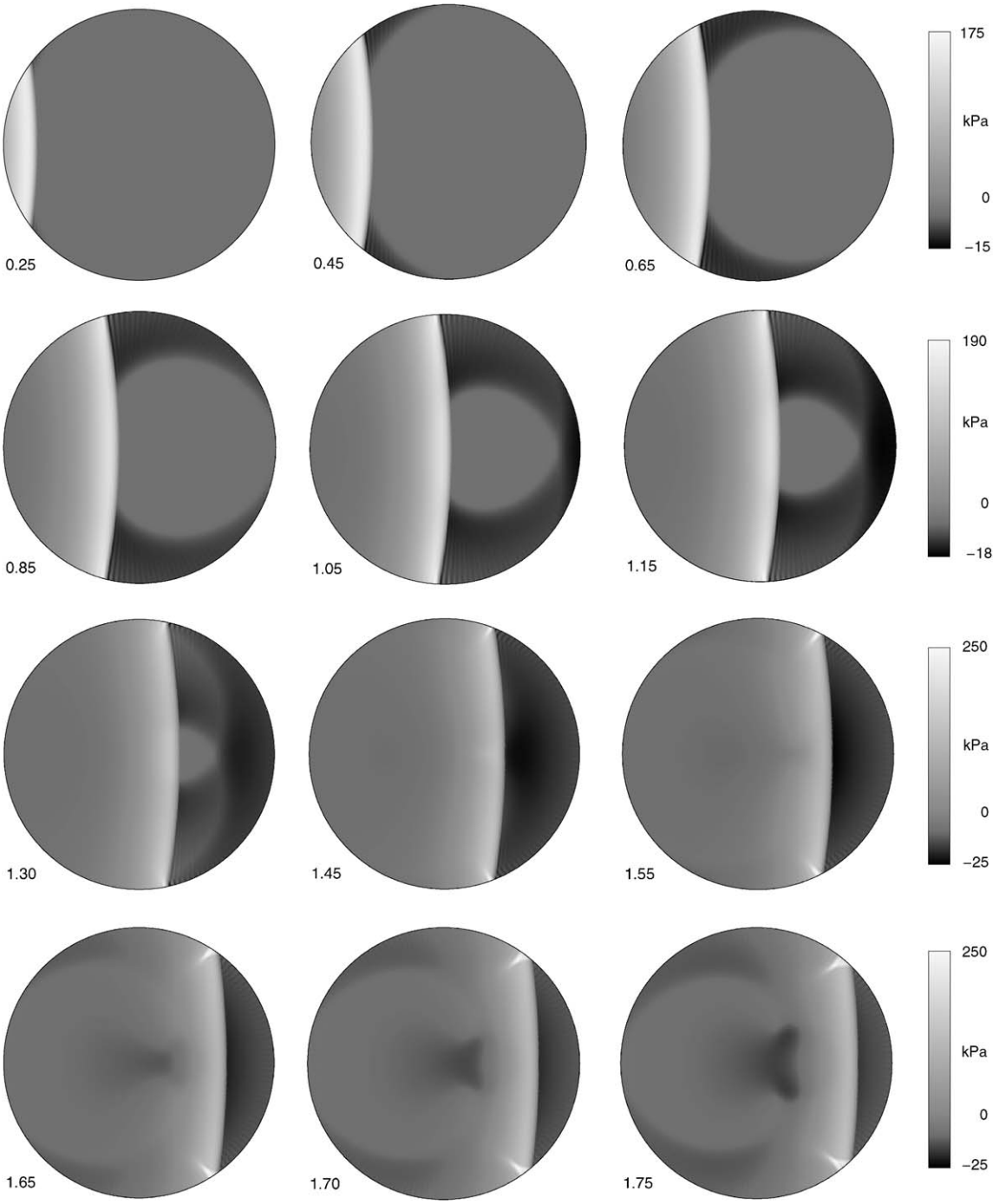

Fig. 3. Downstream propagation of the internal shock wave, $t = 0.25 - 1.75$.

Ben-Dor and Takayama (1992)]. The two zones of high pressure associated with the near-wall formations evolve into a fully developed regular reflection ($t > 1.80$, Figs. 3 and 4), and eventually merge.

We mention that along with the extensive experimental investigation, Sun (1998) and Sun and Takayama (1999) approached the reflection numerically, and observed very good agreement between numerical simulations and experiments. We also mention that, in the actual system, the instant when the near-wall reflection patterns are first observed corresponds to transition from Mach to regular reflection (Sun and Takayama, 1996). It is interesting to point

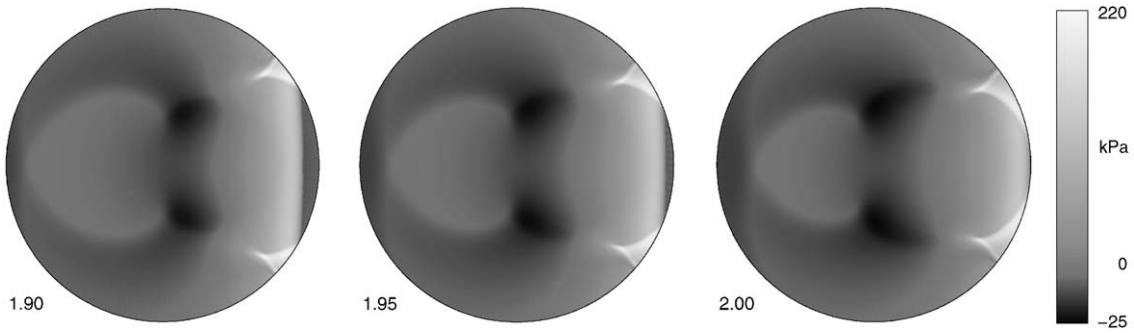

Fig. 4. Downstream propagation of the internal shock wave, $t = 1.90 - 2.00$.

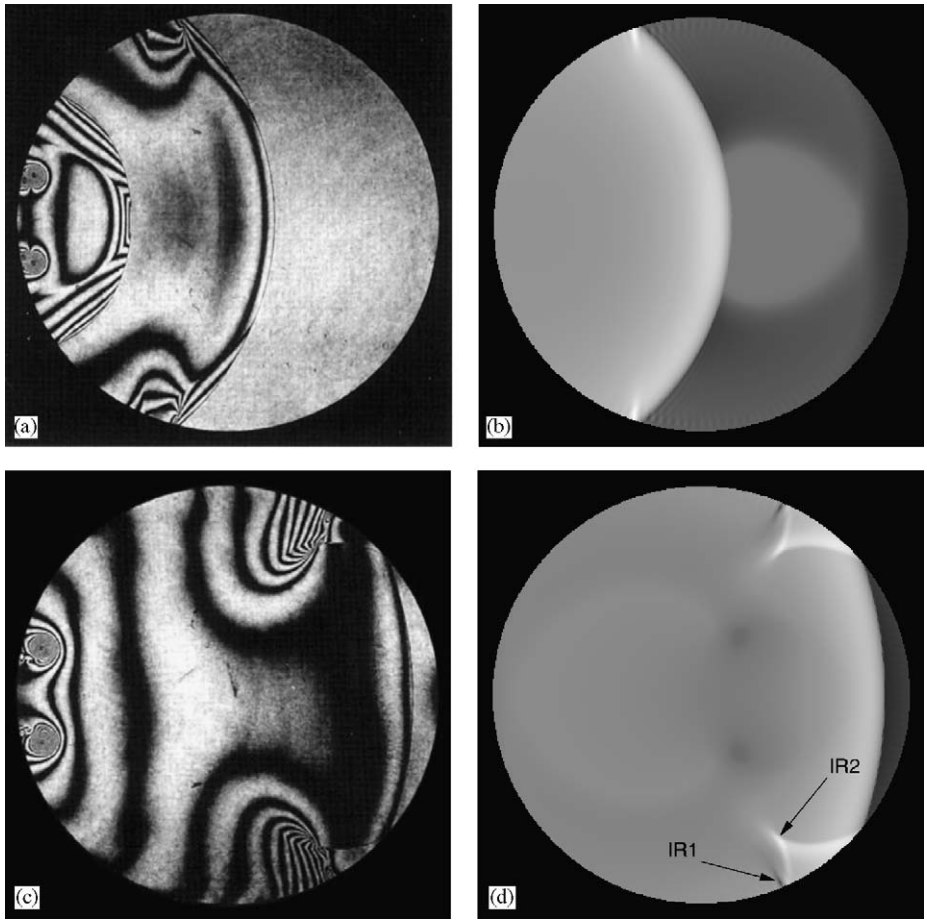

Fig. 5. Comparison of numerically simulated pressure patterns, (b) and (d), versus experimental interferograms, (a) and (c); $t = 1.15$ for (a) and (b), and $t = 1.88$ for (c) and (d). [Interferograms (a) and (c) are reproduced with permission from Sun and Takayama, 1996. A holographic interferometric study of shock wave focusing in a circular reflector, Shock Waves 6, p. 327, Fig. 4(b) and (c), © Springer Verlag 1996].

out that the 'internal' reflection (i.e. reflection from the walls of a circular reflector) is mostly regular, whereas the 'external' one (reflection from a hard cylinder) is mostly Mach. It should be emphasized that the pressure in the regular reflection regions is much higher (up to 65%) than that in the internal shock wave itself, and can be comparable to or even higher than the peak pressure in the incident shock wave. Taking the reflection phenomena in the internal fluid into account is therefore critical for correct estimation of the maximum pressure experienced by the structure.

One can notice that there is a slight difference in the circumferential extension of the regular reflection zones simulated numerically and observed in the experiments. Most likely, this is due to the fact that the experiments were conducted at the Mach number of 1.1, whereas the simulations were carried out for the Mach number of 1.0. The wave pattern observed in the simulated image at $t = 1.15$ in the region that is not yet affected by the internal shock wave is due to the fact that the shell is elastic; this issue is addressed later.

Some secondary features can be clearly identified in both the experimental interferograms and numerical simulations. Specifically, we mention near-wall irregularities (denoted as 'IR1' in Fig. 5(d)) which represent developing secondary regular reflection and later evolve into a clearly identifiable pattern inherent to double regular reflection. Local high-pressure zones IR2 corresponding to the triple points are observed as well. Note that even though the features mentioned are clearly visible in the experimental shadowgrams, the corresponding pressures are hard to quantify. The numerical simulations, however, clearly indicate that the developing secondary regular reflection produces negative pressure, whereas that associated with the triple points is positive. Again, a slight discrepancy in the location of the features discussed is most likely due to the difference in Mach numbers.

The good agreement with the experiments observed allows us to state that for the shock intensities considered, the interior of the shell works mostly as a circular reflector. Even though this is an interesting result, it is not really surprising, since the normal displacements of the shell are much smaller than its thickness in the case considered, and so the interior of the shell is geometrically very close to a circular reflector.

5.2.2. *Shell-induced waves*

We now turn to the analysis of the low-magnitude 'supersonic' waves. These waves represent radiation into the internal fluid of elastic waves propagating in the shell with velocity which is usually much higher than the sound speed in the fluid. The existence of these 'head' waves is a well-known and very important feature of the interaction between elastic shells and high-frequency loads, in particular shock waves. We shall refer to these waves as 'shell-induced' since they are being constantly radiated by the shell, as opposed to the internal shock wave which is originated at the beginning of the interaction, and after that its propagation is mostly governed by acoustic phenomena. Note that the high-frequency low-magnitude pressure oscillations scarcely visible in the plots do not represent any physical phenomena, and appear to be entirely due to series convergence issues.

The overall dynamics of the radiated field is rather uncomplicated. Unlike the positive pressure in the internal shock wave, the shell-induced pressure is negative. This suggests that there is an outward motion of the shell surface associated with the elastic waves, in contrast with its inward motion induced by the incident wave. Analysis of the normal displacements shows that this is indeed the case, even though the magnitude of the corresponding displacements is very small.

The circumnavigating elastic waves reach the tail point at $t = 0.88$ and superpose there, inducing an extensive zone of negative pressure which is considerably lower than that in the shell-induced waves before the superposition. After the superposition, the elastic waves propagate upstream, and continue to contribute to the radiated field. At $t \approx 1.4$ the shell-induced field collides with the internal shock wave, and from then on the entire fluid domain inside the shell is involved in the interaction.

Before proceeding to further analysis, experimental verification of the numerical results obtained seems appropriate. A considerable number of experiments have been carried out to study a variety of waves induced by both short acoustic pulses and steady ultrasonic isonification on submerged and/or fluid-filled shells. Unfortunately, it appears that internal acoustic fields have not been visualized for a cylindrical shell exposed to a normally incident short acoustic pulse. Neubauer and Dragonette (1970) did publish a number of photographs showing the acoustics of the interaction between a submerged fluid-filled shell and an acoustical pulse, but only considered either an angular or partial isonification. Bao et al. (1999) considered an ultrasonic interaction with a fluid-filled submerged shell, but only addressed steady states. Sessarego et al. (1997) analyzed backscattering echo response of a submerged fluid-filled shell to a short acoustic pulse and recorded a sequence of echoes from both circumnavigating and fluid-transmitted waves. Even though they did consider the initial stage of the interaction, the acoustic fields themselves were not discussed. Therefore, it appears that we will have to refer to available experimental studies of more or less closely related systems, and try to show that there is a qualitative agreement between those and numerical results obtained here.

It seems that the most relevant to the present work is the study by Ahyi et al. (1998) who considered a submerged empty cylindrical shell subjected to an ultra-short acoustic pulse and visualized the corresponding shell-radiated waves. Only the initial portion of the first circumnavigation of the pulse was considered, and it appears reasonable to assume that the most important dynamic features of this very early interaction with an acoustic pulse are reasonably close to those observed in the case of the same shell subjected to a weak shock wave. Also, it was shown (Quentin and Talmant, 1989) that the circumferentially propagating waves on fluid-loaded thin cylindrical shells are extremely close to the corresponding waves on fluid-loaded plates (ultra-low frequencies are the only exception due to the fact that the

curvature of the shell starts to have a significant effect; this, however, is not a concern for shock waves). Furthermore, it has been demonstrated (Ahyi et al., 1998) that at the beginning of the interaction, the acoustic field radiated by a plate loaded by fluid on one side is very similar to the field radiated by the same plate loaded by the same fluid on both sides. Therefore, it seems that in the proximity of the shell surface and at the very beginning of the interaction, the internal shell-induced acoustic field in a fluid-filled submerged shell subjected to a weak external shock wave should be qualitatively similar to the external radiated field induced around the evacuated shell by an ultra-short acoustic pulse of similar geometry.

Fig. 6(a) shows an experimental interferogram by Ahyi et al. (1998). Four different types of waves are seen to contribute to the acoustic field around the shell. Along with the incident and diffracted waves (I and SR, respectively), two types of shell-induced waves are observed, the first being a symmetric Lamb wave (A_0), and the second an antisymmetric Lamb wave (S_0). In this work we employ a relatively simple model for the shell, and it does not allow for the observation of all types of elastic waves seen in the experiments. Therefore, we focus our comparison on the S_0 wave.

Fig. 6(b) shows the results of the numerical simulations carried out at $t = 1.20$, which approximately corresponds to the instant the experimental shadowgraph was taken. In both cases, by the time considered, the elastic waves in the shell have propagated around it once, reached the tail point, superposed there, and started to propagate back towards the head point. This elastic process was accompanied by constant radiation of acoustic waves into the fluid, and the shell-induced acoustic field was formed.

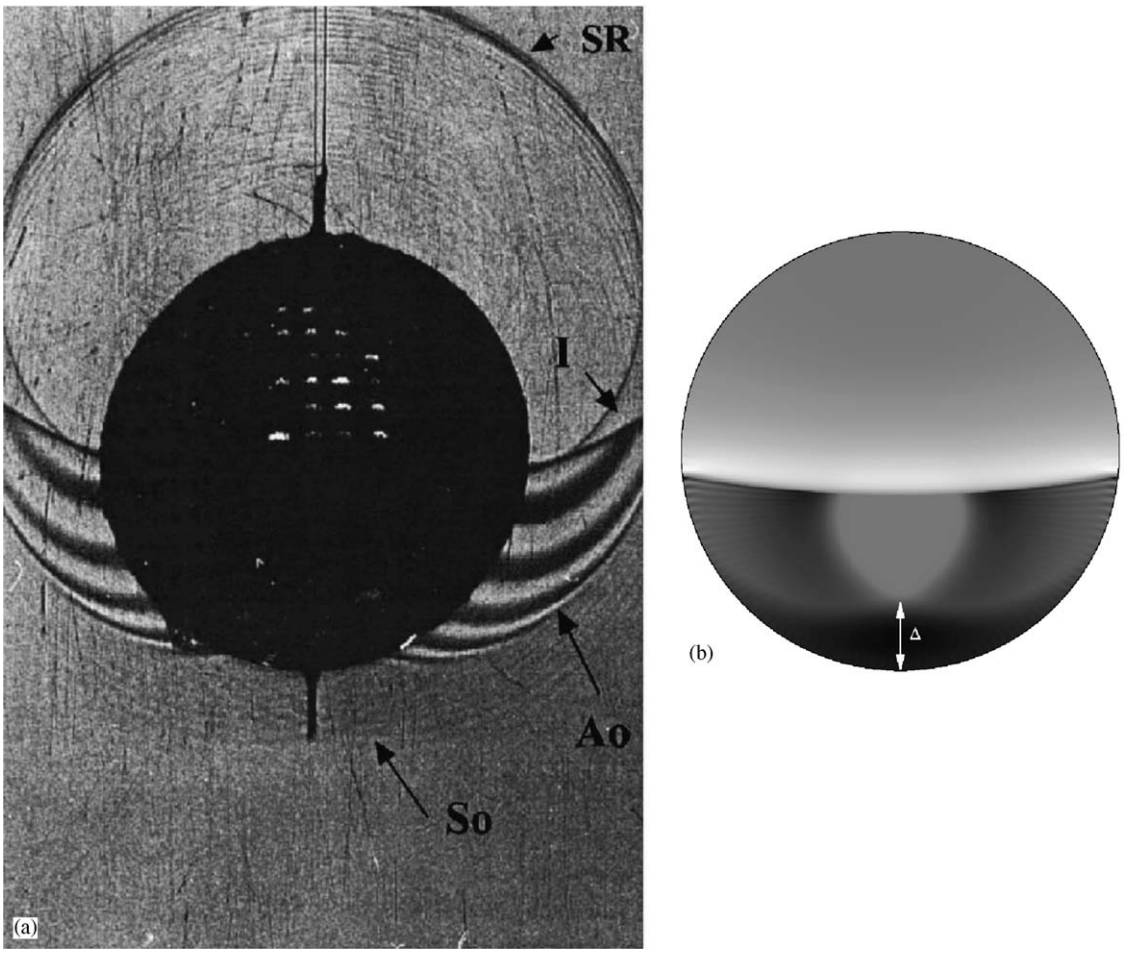

Fig. 6. Comparison of a numerically simulated acoustic field in a submerged fluid-filled shell, (b), to an experimental shadowgraph showing the field around a submerged empty shell, (a); $t = 1.20$ [Shadowgraph (a) is reprinted with permission from Ahyi et al., 1998. Experimental demonstration of the pseudo-Rayleigh (A_0) wave. Journal of the Acoustical Society of America 104, pp. 2727–2732, © American Institute of Physics].

Even though we consider a slightly different steel than that used in the experiments, the radiated wave patterns look very similar in the two cases. Not only is there general qualitative similarity, the upstream circumferential advancement of the corresponding wave fronts is almost the same, approximately 115°. Furthermore, the advancement of the radiated waves at the tail point normally to the shell surface, inward in the fluid-filled case and outward for the submerged shell, is approximately the same in both cases, about 30% of the shell radius (labelled 'Δ' in Fig. 6). Also, the normal advancement of the waves radiated during the first circumnavigation measured at $\theta = 135^\circ$ is almost the same as well, about 60% of the shell radius.

Thus, it appears that the simulations of the shell-radiated field based on the semi-analytical solution obtained here are in a good qualitative agreement with the available experimental data. This fact lends some credence to the physical adequacy of the model employed, since being so much lower in amplitude than the internal shock wave, the shell-induced waves are probably the most 'delicate' physical feature of the interaction, and are therefore more difficult to model than the internal shock wave itself.

Having observed a good qualitative agreement with experiments, we look at shell-induced waves at larger times. The next few superpositions of these waves travelling around the shell occur at 1.76 (head point), 2.64 (tail point), 3.52 (head point), and 4.40 (tail point). Even though it was very easy to observe the acoustic effect of the superposition after the first circumnavigation, detecting superpositions at larger times becomes more difficult due to multiple wave interferences inside the shell, and also because the amplitude of shell-induced waves decreases with time. However, the superposition of the waves that travel around the shell only once and return to the head point at $t = 1.76$ can still be easily observed, Fig. 7. Note that the geometry of the radiated field in this case is quite similar to that of the field observed during the first superposition at the tail point.

The superposition at the tail point at $t = 2.64$ is not observable due to the fact that it coincides with the much higher-magnitude process of reflection and focusing of the internal shock wave. However, later superpositions can still be observed, even though the associated pressures are low. The radiated fields induced by those late superpositions are very similar to what we have already seen, and the corresponding pressure plots are not shown.

Finalizing the discussion of the shell-induced waves we mention an experimental study of the interaction between a spherical shock wave and an elastic spherical body (Merlen et al., 1995; Latard et al., 1999), and a numerical study in which a submerged elastic cylinder subjected to a shock wave was considered (Takano et al., 1997). Even though the physics of such shock–solid interaction is quite different from the case considered here, it is worth mentioning that the solid-induced 'head waves' propagating with a supersonic (relative to the fluid) velocity were reported in those publications as well.

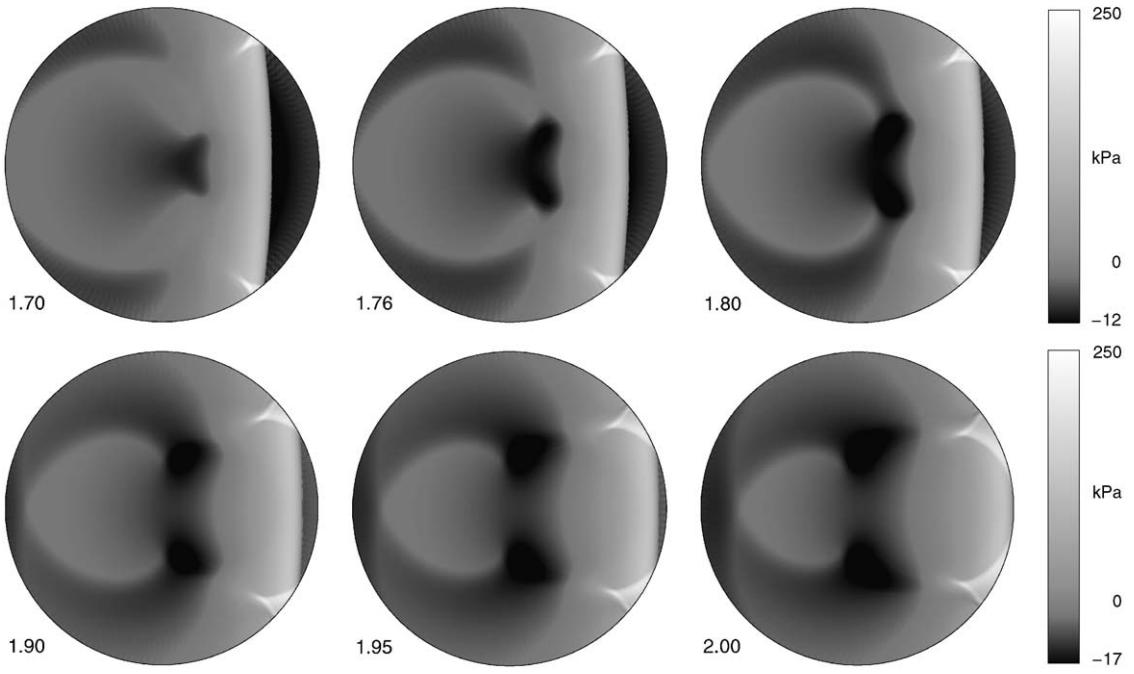

Fig. 7. Acoustic field induced by the superposition of the elastic waves at the head point at $t = 1.76$.

5.3. Primary reflection and focusing

After the internal shock wave reaches the tail region, it is reflected from the shell surface, and shortly after that the reflected wave focuses, Figs. 8 and 9. Note that even though the internal shock wave reaches the tail point at exactly $t = 2.00$, due to the fact that it does not have a front, the pattern inherent to shock wave diffraction, i.e. a significant

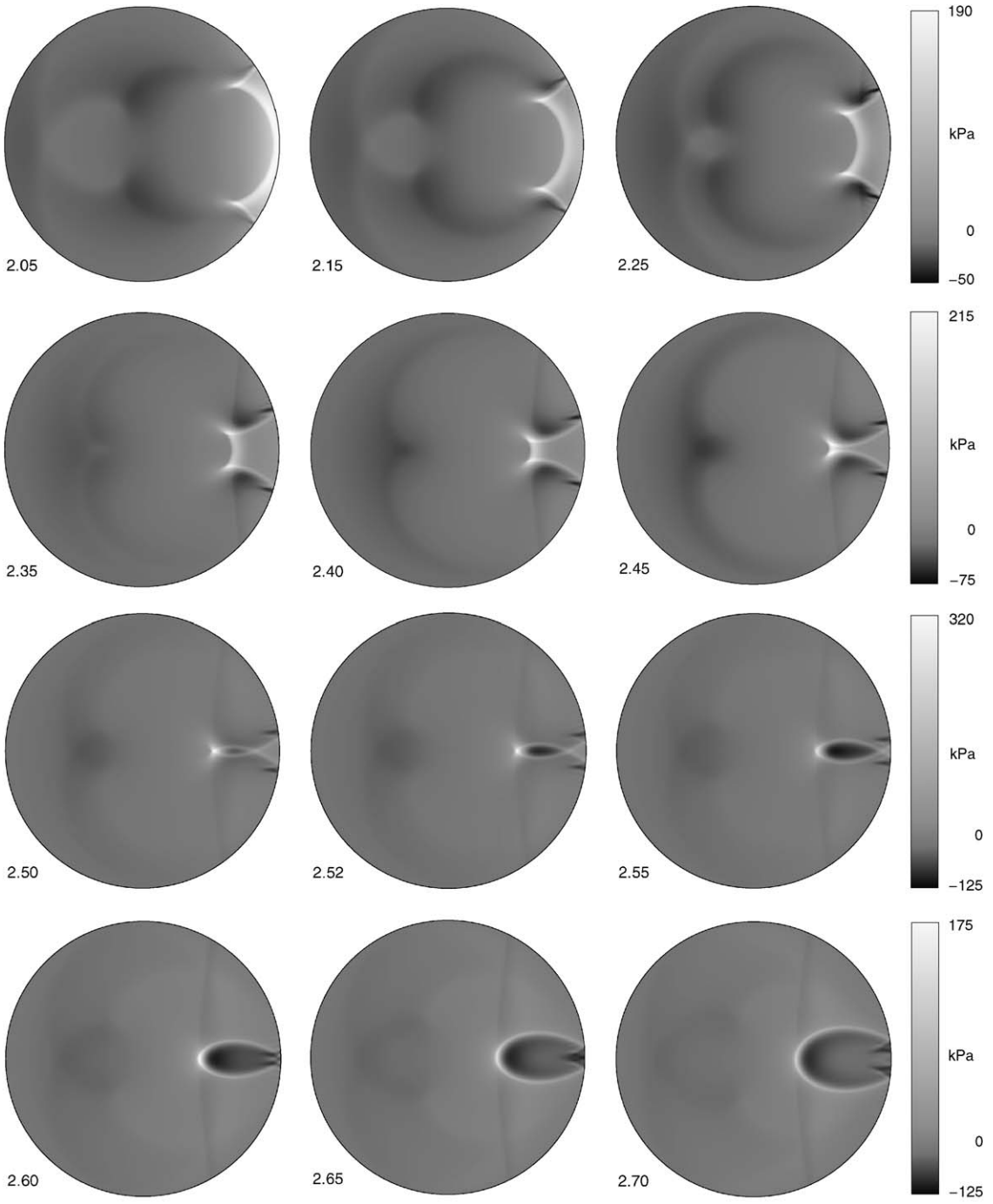

Fig. 8. Reflection and focusing of the internal shock wave, $t = 2.05 - 2.70$.

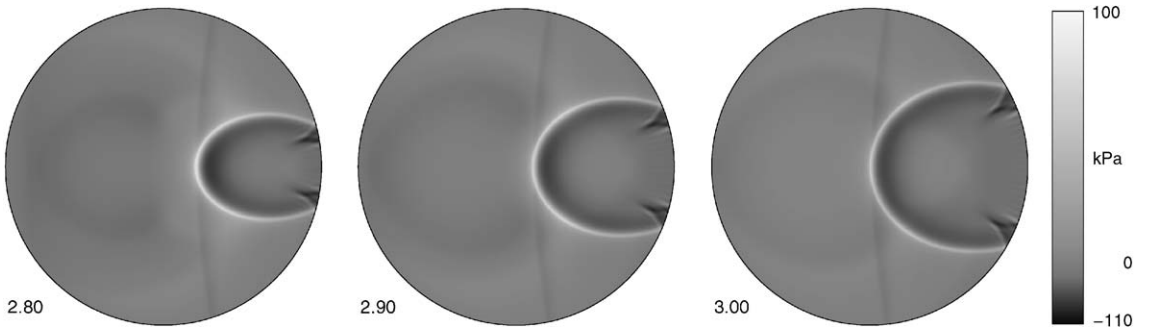

Fig. 9. Reflection and focusing of the internal shock wave, $t = 2.80 - 3.00$.

increase of pressure at the reflection point, is observed with a slight delay of $\Delta t \approx 0.03$. Even though the difference between the 'classical' shock reflection scenario and the present case is negligible, it is worth reporting, since it clearly demonstrates the fact that there is no pressure discontinuity associated with the internal pressure wave. There are a number of other interesting dynamic features observed during reflection and focusing. Before we discuss those, we compare our numerical simulations with available experimental results. Once again, we refer to the experiments by Sun and Takayama (1996).

Fig. 10(a) and (b) shows comparison between the simulated and experimentally observed pressure fields right before focusing ($t = 2.53$). A very good overall agreement is observed, including several secondary features of the pressure patterns. Of those, we mention the symmetric high-pressure regions F1 corresponding to the triple points, Mach stems F2, and the secondary regular reflection that has developed along the wall, F3. The latter is a very interesting shock wave reflection phenomenon. Namely, it is known that regular reflection may repeat itself many times to produce a series of reflection patterns (Sun and Takayama, 1996; Sun, 2004). As we will see shortly, the present case exemplifies such a scenario, and a number of self-similar regular reflection patterns develop later in the interaction. It is interesting to point out that, while the primary regular reflection produces positive pressures, the secondary regular reflection produces negative ones. Note that there is a low-magnitude wave of negative pressure F4 which is present in the simulated plots but is not seen in the experimental interferogram. This issue is addressed later. Note also that the blurriness of the numerically generated pressure patterns is due to both the discussed features of the internal shock wave and certain computational limitations (pressure was computed in 100 'layers' r-wise, and interpolation was used for points between the layers).

Another comparison we consider is that of the pressure patterns right after the focusing, $t = 2.67$, Fig. 10(c) and (d). Again, a good overall agreement is observed, including the well-developed double regular reflection F5a and F5b and very high-magnitude 'tip' F6. As was the case with the pre-focusing field, the low-magnitude pressure wave F7 is observed numerically but not experimentally.

Having observed a good agreement between the numerical results and experiments, we proceed to further discussion of the reflection and focusing. First of all, we address the 'secondary' low-magnitude reflected wave (F4 and F7) which is not seen in the experimental interferograms. Note that this reflected wave is present in the large-stand-off case as well, Figs. 8 and 9; it is apparent that the reflected waves have different curvatures in the small- and large-stand-off cases.

Since the only difference between a circular reflector and the present case is the elasticity of the shell walls, it seemed logical to assume that the secondary reflected wave is a product of the shell motion caused by the reflection of the internal shock wave from the tail region. This, however, is not the case. Indeed, we have just seen that the two wavefronts of different curvature produce different secondary reflected waves. Therefore, if those waves were 'elastic' in origin, shell velocity profiles simulated for two different curvatures of the incident wave would have to differ in the tail region quite significantly as well. This, however, does not happen, and it can be shown that the shell velocity distribution in the tail region at the time of reflection is very similar for both the small- and large-stand-off incident waves. This suggests that the secondary reflected waves are acoustic in nature, or at least are not directly induced by the motion of the shell surface.

Careful analysis of the reflection revealed that these secondary waves indeed are present due to the fact that the shell is elastic. However, their physics is more complex than was initially thought. To understand what is happening, we recall that shell-induced waves of negative pressure are propagating in the internal fluid well ahead of the internal shock wave. In particular, we have seen that after the superposition of the elastic waves at $t = 0.88$ at the tail point, a zone of negative pressure starts to develop in the proximity of the tail region, and eventually it propagates upstream. At the

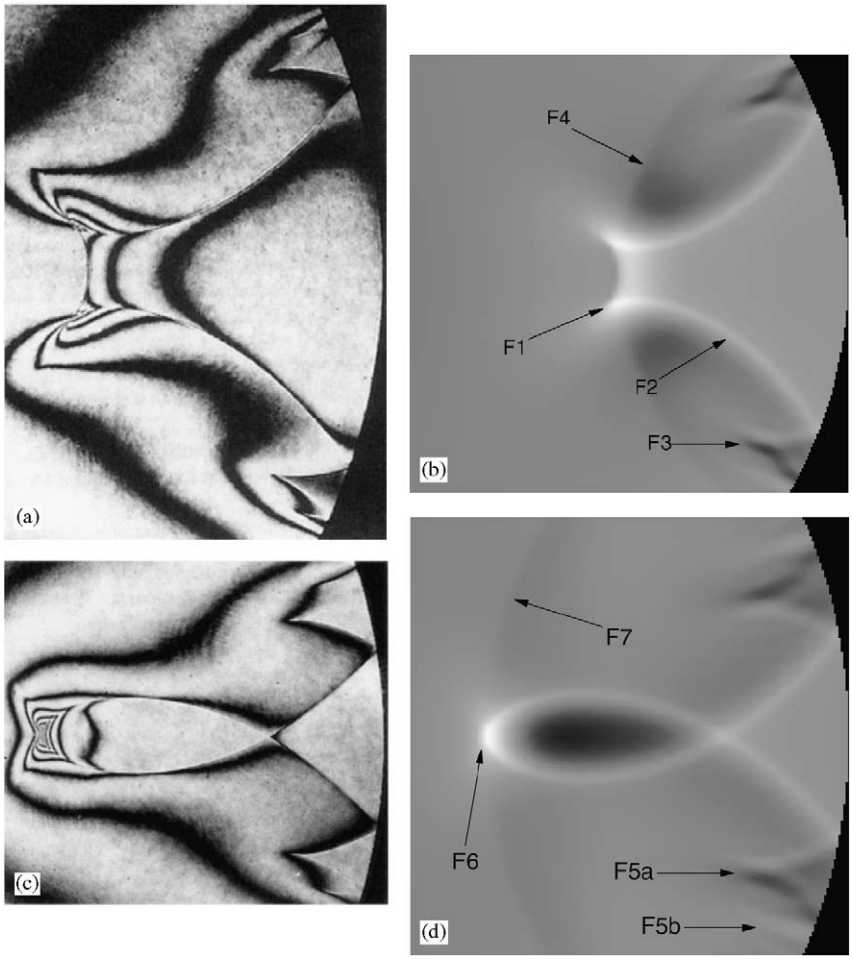

Fig. 10. Comparison of numerically simulated pressure patterns, (b) and (d), versus experimental interferograms, (a) and (c); $t = 2.53$ for (a) and (b), and $t = 2.67$ for (c) and (d) [Interferograms (a) and (c) are reproduced with permission from Sun and Takayama, 1996. A holographic interferometric study of shock wave focusing in a circular reflector. Shock Waves 6, p. 335, Fig. 12(a) and (b), 1996, © Springer-Verlag 1996].

same time, the internal shock wave propagates downstream, and the two wavefronts collide at $t \approx 1.4$. After that, the internal shock wave continues to propagate downstream. However, the pressure in the area which is not yet affected by this wave is not zero anymore, it is *negative*. So, effectively, one observes a low-magnitude zone of negative pressure that decreases in size and eventually collapses at $t = 2.0$. This collapse apparently results in a wave of negative pressure we refer to as the 'secondary reflected wave'.

Since the shape and size of the negative pressure zone is completely determined by the curvature of the internal shock wave, the explanation proposed rests well with the observed geometrical differences of the reflected waves in the small- and large-stand-off cases. It should be emphasized that the existence of such a wave of negative pressure appears to be a unique feature of the interaction between an *elastic* shell and an external shock wave.

We note that in the original high-resolution photographs (Sun, 2004), a secondary reflected wave with the geometry very similar to the one observed here is scarcely visible right after the reflection. However, it is not present in the images at later instants. This fact leaves some room for further discussion of the numerically observed secondary reflected wave. To clarify the issue completely, one would have to use the present linear model and simulate the reflection from the interior of the shell of the same geometry under the assumption of absolute rigidity of the walls. That, however, would require one to consider an internal explosion, in which case multiple reflections from the shell surface would significantly complicate analysis of the acoustic field.

Now we turn to another interesting aspect of the interaction. Namely, it is known that focusing of a shock wave produces high pressures. The magnitudes of those are always of particular practical interest. It turns out that in the considered case of a large-stand-off shock wave, the maximum positive pressure produced by focusing reaches 320 kPa at $t \approx 2.50$. This pressure exceeds the peak incident one by almost 30%, and is about two times higher that the maximum pressure in the internal shock wave in the beginning of the interaction. Moreover, focusing is followed by relatively high-magnitude negative pressure. In the present case, it can be as low as -140 kPa at $t \approx 2.64$, which corresponds to 55% of the peak incident pressure.

From the practical point of view, the observations made imply that the engineer should be prepared to deal with internal pressures that are comparable to or even higher than the peak pressure in the incident shock, and which occur *after* the incident wave has passed over the structure. This observation is of particular importance when one analyzes safety of shell structures containing interior elements, especially if those are shock-sensitive (e.g., thin-walled pipes, various equipment etc.). It is important to note that if such interior elements are present, the pressure pattern in the internal fluid will change, and, strictly speaking, the results obtained here would no longer be valid. However, if the interior elements in question occupy a relatively small volume, and if they are not located in the close proximity of the focal point, the results presented will probably still be applicable. An earlier study of the stress–strain state of a fluid-filled shell containing a rigid cylindrical core (Iakovlev, 2004) seems to support this conclusion, even though the acoustics of such a system is yet to be studied.

5.4. Upstream propagation and secondary reflection and focusing

To the best of the author's knowledge, the upstream propagation of the reflected internal shock wave has not been addressed either experimentally or numerically. Phan and Stollery (1985) considered upstream propagation in a circular reflector and visualized reflection of an internally generated shock wave from a plane internal wall. However, such a system is very much different from the one considered here, and is of little use when one is concerned with a shell with no interior structures attached to it subjected to an external shock wave.

Despite the lack of literature addressing the late interaction, it appears to be of theoretical and practical interest. In particular, we shall show that this stage has some rather unique dynamic features which are not observed during the earlier interaction. We shall also demonstrate that secondary focusing produces very low pressures comparable in magnitude with the maximum positive pressures in the very beginning of the interaction. Furthermore, analysis of the late interaction is of interest since at such large times the influence of the incident shock wave is negligible for any practically meaningful decay rate, and so the process is almost completely driven by the wave phenomena in the shell and fluid(s).

Figs. 11 and 12 show a sequence of pressure snapshots during the upstream propagation. First of all, we reiterate the fact that there are two reflected shock waves of different magnitudes propagating in the fluid. The 'primary' wave has an elliptically shaped front originated after the collapse of the triple points. The origins of the 'secondary' one were discussed earlier, and the front of this wave has a much larger radius of curvature. Interacting with the shell surface, the secondary reflected wave follows a reflection pattern which is very similar to that of the internal shock wave during the downstream propagation. The primary reflected wave, however, exhibits completely different dynamic features.

Initially ($t \approx 3$), the interaction of the 'front' of the primary reflected wave with the shell surface produces the classical single regular reflection pattern. Later, however, another regular reflection starts to develop at a smaller scale at the foot of the primary Mach stem ($t = 3.20 - 3.60$). This process is repeated over and over again, with self-similar regular reflections originating at smaller scales. Eventually, one can observe as many as three self-similar regular reflection patterns, e.g., $t = 4.85 - 5.00$. The possibility of such multiple reflection patterns has been discussed in the literature [e.g., Sun and Takayama (1996), Sun (2004)], and it is of interest to actually see it develop.

Even though the primary and secondary reflected waves have different curvatures, they propagate through the fluid with the same velocity, and both reach the head point at $t = 4.00$. The secondary wave reflects from the head region and focuses; the corresponding pressure patterns are very similar to those observed for the internal shock wave in the proximity of the tail region at $t > 2$. The reflection pattern of the primary reflected wave is different due to a different geometry of its front. We note that due to a significant difference in magnitudes, the reflection pattern of the secondary wave 'underlies' that of the primary one and appears in Figs. 11 and 12 as a scarcely visible 'ghost image'.

The secondary focusing occurs at $t \approx 4.74$ and it produces high-magnitude negative pressure, as opposed to the high-magnitude positive pressure produced by the primary focusing. It is of particular interest that the global minimum of the pressure is reached during the secondary focusing. The pressure drops below -150 kPa, i.e. it is even lower than the minimum attained shortly after the primary focusing. This fact has some interesting implications when cavitation is a

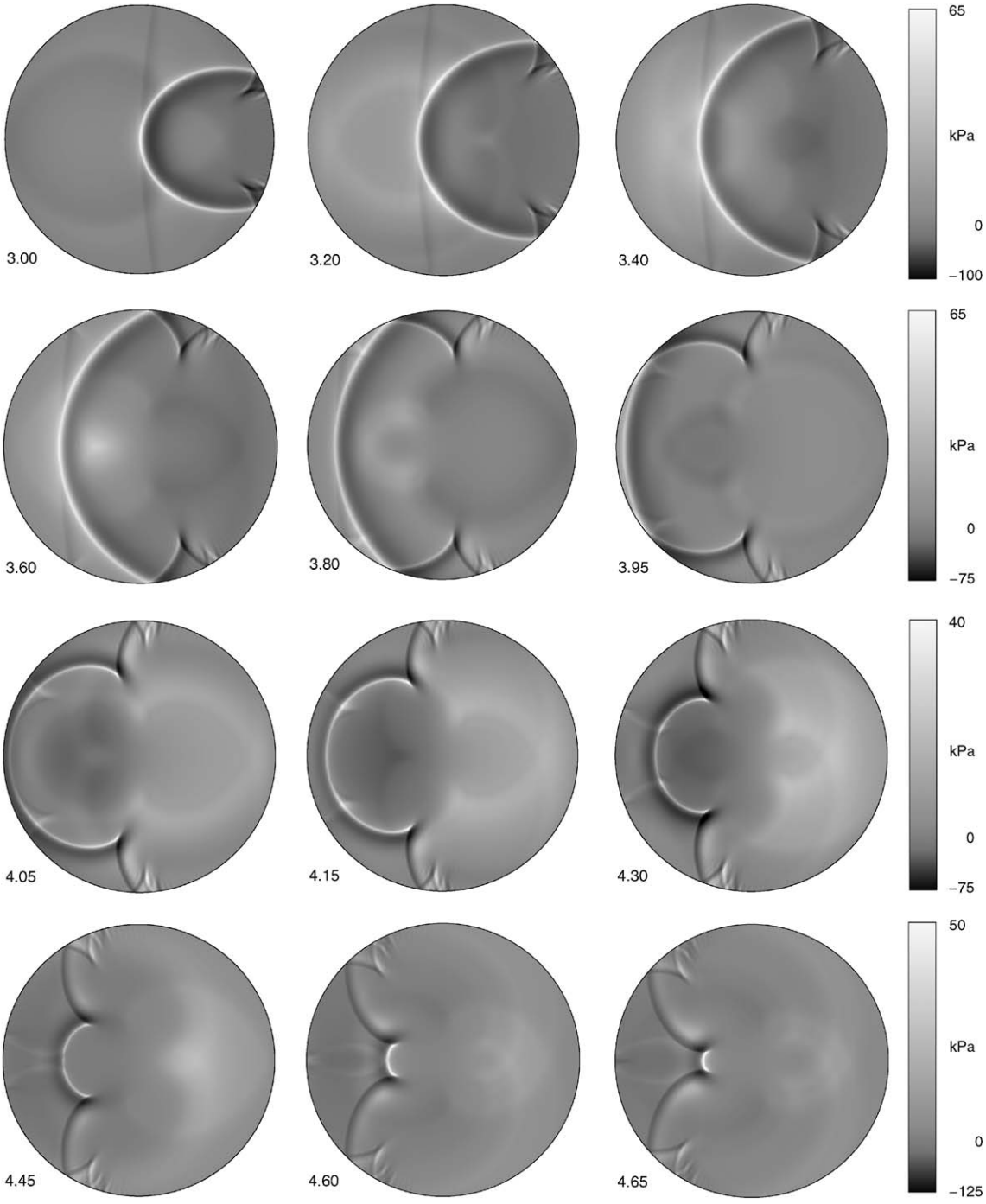

Fig. 11. Upstream propagation of the internal shock wave, $t = 3.00 - 4.65$.

concern. We emphasize that for the shell considered, the low pressure observed during the secondary focusing is equal in magnitude to the maximum pressure in the internal shock wave in the beginning of the interaction. We also note that after the secondary focusing, the internal wave pattern becomes rather complex due to the well-developed multiple regular reflection.

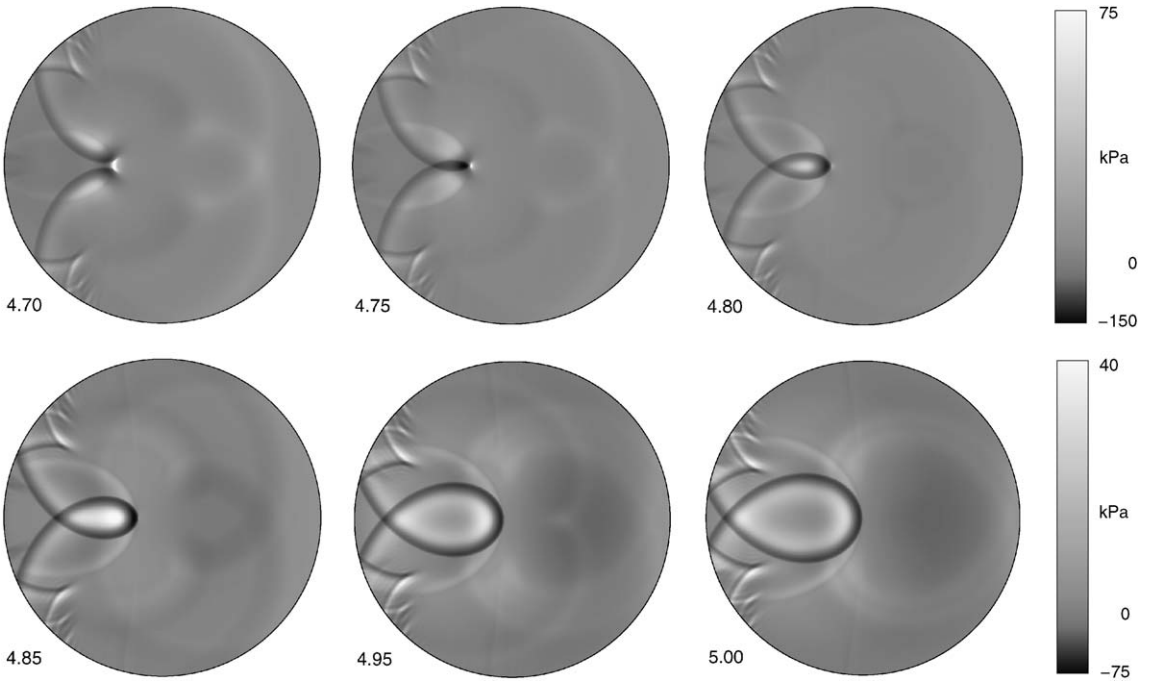

Fig. 12. Upstream propagation of the internal shock wave, $t = 4.70 - 5.00$.

6. Conclusions

We have considered the interaction between a submerged fluid-filled circular cylindrical shell and an external shock wave, and focused our study on the internal acoustic field. A fully linear model of the system was employed, and a semi-analytical solution was obtained. The interaction was simulated numerically and the internal acoustic field was visualized.

A very good agreement between the numerically simulated pressure fields and available experimental data was observed. In particular, it was found that the wave propagating in the internal fluid exhibits all the major dynamic features inherent to shock wave reflection from curved surfaces, as well as some of the secondary features; namely, well-developed regular reflection and the associated Mach stems and triple points were observed, as well as the focusing of the reflected wave. The low-magnitude shell-radiated waves which are an important feature of any fluid–structure interaction were also observed. It is possible, therefore, to state that a relatively simple, completely linear model employed in this work captures the complex dynamics of the interaction really well.

From the physical point of view, a close similarity between the simulated pressure fields inside an elastic shell and experimental results for rigid-wall reflectors implies that when the incident shock wave is relatively weak, the interior of the shell works as a circular reflector with respect to the wave propagating in the internal fluid. Furthermore, a good agreement with experimental data suggests that the solution obtained is suitable for use as a benchmark. It also suggests that the methodology employed in this work can be confidently used to study more complex fluid-interacting shell systems, in particular those for which experimental data is not yet available.

Along with qualitative analysis of the interaction, the pressure inside the shell was also quantified. In particular, it was found that the peak pressure produced by the focusing of the internal wave can be substantially higher than the peak incident pressure. For a shell with the thickness-to-radius ratio of 0.01, for example, the maximum focusing pressure exceeds the peak incident one by almost 30%. From the engineering point of view, this observation is of particular importance when shock-sensitive elements are placed inside a fluid-filled shell. The study of the reflection and focusing has also demonstrated that analysis of the pressure distribution on the shell surface is not sufficient to account for the acoustic features of the entire system. Some important acoustic phenomena take place inside the fluid, and manifest themselves on the shell surface with a sometimes considerable delay.

The late interaction was addressed as well, i.e. the dynamics of the system was analyzed well after the incident shock wave has passed over the shell. In spite of the fact that very limited information is available in the literature on this stage of the process, it exhibits some very interesting wave reflection phenomena. In particular, multiple regular reflection was seen to develop along the surface of the shell, and up to three self-similar regular reflection patterns could be clearly identified.

The internal pressure was expressed in terms of the normal displacement of the shell surface and what we referred to as the 'volume response functions'. From the experimentalist's point of view, such a representation suggests a possibility of using the experimental measurements of the normal displacement to simulate the entire internal acoustic field. Since such measurements are less technically challenging than recording the dynamics of the acoustic field itself, exploring this possibility seems to be an interesting direction for the future research.

In summary, we state that the fully linear approach employed in this work appears to be working quite well. Not only can it be used to understand the physics of the interaction between shock waves and shell systems that are more complex than the one considered here, it can also be employed to produce a series of fluid–structure interaction benchmark solutions.

Acknowledgements

The author gratefully acknowledges the financial support of the Natural Sciences and Engineering Research Council (NSERC) of Canada (Discovery Grant 261949), the Killam Trusts at Dalhousie University, and the Faculty of Engineering, Dalhousie University. The author is also grateful to Dr. Mingyu Sun of the Institute of Fluid Science, Tohoku University, Sendai, Japan, for sharing results of his experimental work and for granting permission to reproduce them in this publication, and to Dr. Ayayi Claude Ahyi of the Auburn University, Alabama, USA, for granting permission to reproduce a photograph from one of his publications. The assistance of Mr. Mathew P. Bligh, a Mechanical Engineering student at Dalhousie University, is appreciated as well.

Appendix A. Internal response functions

In order to obtain the response functions $\xi_n^i(r,t)$, we employ the same analytical procedure as the one that was used to compute their 'surface' counterparts $\psi_n^i(t)$ [the procedure itself, along with all necessary proofs, can be found in Iakovlev (2002b)]. Since the inversion technique remains very much the same, we will just briefly outline the highlights, and then focus on the results and the difference brought in by the space variable r.

It can be shown that all zeros of the denominator of (30) are pure imaginary, of first order, and are given by

$$s_{\pm k}^n = \pm\omega_k^n, \quad k = 1, 2, \ldots, \tag{51}$$

where ω_k^n is the kth positive zero of the first derivative of the Bessel function of first kind of order n, J_n, except for the point $s = 0$. Ξ_n^i therefore has an infinite number of simple poles given by (51), with the point $s = 0$ being a second order pole for $n = 0$ and a removable singular point for $n \geqslant 1$.

It can also be shown that Mellin's integral for Ξ_n^i,

$$\xi_n^i(r,t) = \frac{1}{2\pi\mathrm{i}} \int_{\varepsilon-\mathrm{i}\infty}^{\varepsilon+\mathrm{i}\infty} \Xi_n^i(r,s)\ \mathrm{e}^{st}\,\mathrm{d}s, \tag{52}$$

where ε is such that all the singular points of the integrand

$$Z_n(r,s) = \Xi_n^i(r,s)\ \mathrm{e}^{st} \tag{53}$$

lie in the half-plane $\mathrm{Re}\, s < \varepsilon$, can be expressed in terms of the residues of the integrand at the poles (51) and possibly the point $s = 0$. Then, the functions $\xi_n^i(r,t)$ can be obtained as

$$\xi_n^i(r,t) = \sum_{k=\pm1,\pm2,\ldots} R_{s_k^n}^n, \tag{54}$$

where $R_{s_k^n}^n$ is the residue of $Z_n(r,s)$ at the point $s = s_k^n$.

The residues can be obtained as

$$R_0^0 = 2t, \tag{55}$$

$$R^n_{i\omega^n_k,\,k=1,2,\ldots} = \frac{J_n(r\omega^n_k)}{J_n(\omega^n_k)} \frac{i\omega^n_k}{\{n^2-(\omega^n_k)^2\}} \{\cos(\omega^n_k t) + i\,\sin(\omega^n_k t)\}, \tag{56}$$

and

$$R^n_{-i\omega^n_k,\,k=1,2,\ldots} = -\frac{J_n(r\omega^n_k)}{J_n(\omega^n_k)} \frac{i\omega^n_k}{\{n^2-(\omega^n_k)^2\}} \{\cos(\omega^n_k t) - i\,\sin(\omega^n_k t)\}, \tag{57}$$

and hence $\xi^i_n(r,t)$ is given by

$$\xi^i_0(r,t) = 2t + 2\sum_{k=1}^{\infty} \frac{J_0(r\omega^0_k)}{J_0(\omega^0_k)} \frac{1}{\omega^0_k} \sin(\omega^0_k t), \tag{58}$$

and

$$\xi^i_n(r,t) = 2\sum_{k=1}^{\infty} \frac{J_n(r\omega^n_k)}{J_n(\omega^n_k)} \frac{\omega^n_k}{\{(\omega^n_k)^2-n^2\}} \sin(\omega^n_k t), \quad n \geqslant 1. \tag{59}$$

Note that upon substitution of $r=1$ into (58) and (59) we arrive at the analytical expressions for ψ^i_n (Iakovlev, 2002b), which of course is expected since the 'surface' response functions are just a special case of the 'volume' ones. Despite the similarity between the analytical expressions for the 'surface' and 'volume' response functions, the latter are significantly more complex. We will discuss the most important aspects of this complexity.

First of all, we mention that as it was the case with ψ^i_n, the functions ξ^i_n have infinitely many points of discontinuity which are of two types, singularities and finite discontinuities. However, the number of discontinuities of ξ^i_n in any given t-interval is different than that of ψ^i_n. Moreover, unlike in the 'surface' case, locations of the discontinuities are not fixed at the points $t=2, 4, 6$, etc. Specifically, they depend on r, and the singularities are located at $t = 1+r, 3-r, 5+r$ etc., i.e. at the points

$$t^s_m = 2m + 1 + (-1)^m r, \quad m = 0, 1, \ldots, \tag{60}$$

whereas the finite discontinuities are located at the points $t = 1-r$, $3+r$, $5-r$ etc., i.e. at

$$t^f_m = 2m + 1 - (-1)^m r, \quad m = 0, 1, \ldots\ . \tag{61}$$

As an example, Fig. A.1 shows the function $\xi^i_1(r,t)$ for various r. Note that (60) and (61) are applicable to the 'surface' case $r=1$ as well, but in that case each point of discontinuity is represented by two equal consecutive values given by these equations (e.g., $1+r$ and $3-r$ will produce the first singular point of ψ^i_n at $t=2$, whereas $3+r$ and $5-r$ correspond to its first point of finite discontinuity at $t=4$). Note that the value of ξ^i_n at a point of finite discontinuity is

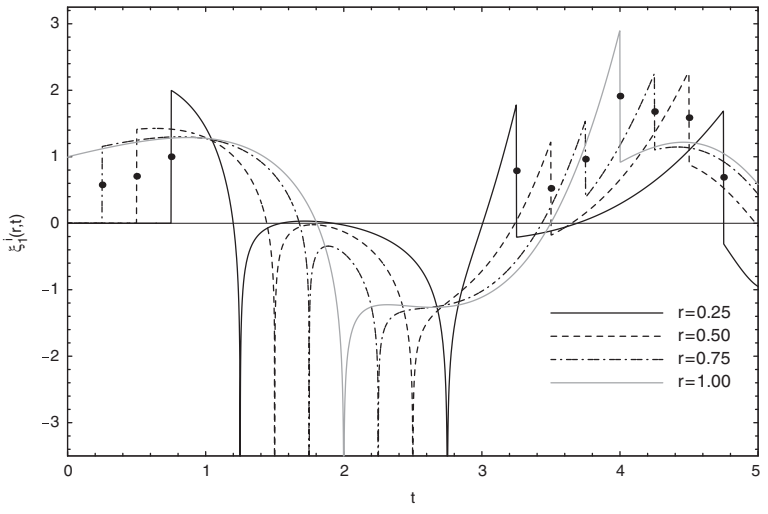

Fig. A.1. Response function $\xi^i_1(r,t)$ for various r.

equal to a half of the sum of the left- and right-side limits at that point [the phenomena discussed in Iakovlev (2002b)], and is represented by dots in Fig. A.1. To avoid making the plots overly complex, the functions in Figure A.1 are shown as continuous.

Before we turn to analysis of the physics behind the discontinuities, we note that $\xi_n^i(r,t)$ represent the response of the internal fluid to the sudden motion of the shell surface with the velocity numerically equal to $\cos n\theta$. Indeed, if we rewrite (39) as

$$\hat{p}_n^{r,i} = -\dot{w}_n(t-\eta)\xi_n^i(r,\eta)|_0^t + \int_0^t \dot{w}_n(t-\eta)\dot{\xi}_n^i(r,\eta)\,\mathrm{d}\eta, \tag{62}$$

where a dot over a function denotes its first derivative, and assume that $\dot{w}_n(t)=1$ for all $t>0$ and $\dot{w}_n(0)=0$ (i.e. that the shell surface suddenly starts to move at $t=0$ with the velocity of $\cos n\theta$), the pressure radiated by the shell into the internal fluid will be given by

$$\hat{p}_r^i(r,\theta,t) = \xi_n^i(r,t)\cos n\theta \tag{63}$$

for $r<1$, and

$$\hat{p}_r^i(1,\theta,t) = \{\xi_n^i(1,t)+1\}\cos n\theta. \tag{64}$$

The pressure on the inner surface of the shell and inside the fluid is governed by different equations since every time the wave contacts the shell, the pressure increases by unity (multiplied by the cosine factor). If we set $\theta=0$, i.e. consider the pressure distribution along the centreline, response functions at the point $(r,0)$ become numerically equal to the radiation pressure at that point, and so the underlying physics becomes particularly easy to understand.

Iakovlev (2004) hypothesized about the physical origins of the two types of discontinuities observed, and suggested that the singularities represented 'focusing' of internal acoustic waves at the centre $r=0$, whereas the finite discontinuities were attributed to reflection of the acoustic waves from the internal surface(s) (note that the words 'reflection' and 'focusing' are used here not in a shock wave sense but in the context of the above-discussed axisymmetric pressure wave which converges at the centre and reflects from the walls). The explanations proposed in Iakovlev (2004) seem to be further supported in most parts by the results obtained here, with some clarifications to be made.

To see what is actually happening inside the shell, we assume that its surface is moving according to

$$\frac{\partial w}{\partial t} = \cos n\theta, \quad t>0, \quad \left.\frac{\partial w}{\partial t}\right|_{t=0} = 0, \tag{65}$$

and observe the pressure at the point $(r,0)$. The initial pressure impulse propagates through the internal fluid and reaches the centre at $t=1$ where focusing occurs producing a pulse of infinite pressure. At the point $(r,0)$ this pulse will be detected at $t=1+r$, which correspond to the first singular point of ξ_n^i. At the same point, the original impulse itself propagating towards the centre will be detected at $t=1-r$, and since the pressure corresponding to that impulse is finite, $t=1-r$ is a point of finite discontinuity for ξ_n^i.

After the focusing occurs, the infinite pressure pulse travels back towards the shell surface where it reflects at $t=2$ (which corresponds to the first singularity of the 'surface' response function ψ_n^i). After that, it travels back to the centre. As a result, at the point $(r,0)$ an infinite pressure is detected again at $t=3-r$, which corresponds to the second singular point of ξ_n^i. At $t=3$, infinite pressure pulses arrive at the centre simultaneously from all directions and focus there which results in a finite pressure pulse. It travels towards the shell surface, and passes through the point $(r,0)$ at $t=3+r$ which corresponds to the second finite discontinuity of ξ_n^i. This finite pressure pulse reaches the shell surface at $t=4$ (which corresponds to the first finite discontinuity of the 'surface' response function ψ_n^i), reflects from it, and travels back to the centre passing through the point $(r,0)$ at $t=5-r$ which corresponds to the third finite discontinuity of ξ_n^i. Then the finite pulse focuses at the centre at $t=5$ resulting in an infinite pressure pulse, and the process continues with the 'finite–infinite–infinite–finite' pulse sequence being continuously repeated.

Thus, we have established that, as was the case with the 'surface' response functions, the singular points of ξ_n^i represent focusing of the internal wave at the centre. As to the finite discontinuities, some remarks are to be made. For all $r<1$, the first finite discontinuity of ξ_n^i corresponds to the compression wave originated at $t=0$ on the shell surface. All other finite discontinuities correspond to focusing of infinite pressure pulses at the centre which results in finite pressure pulses. Since this is only possible when an infinite pulse reflects from the shell surface and reaches the centre, it still makes sense to attribute the finite discontinuities, except for the first one, to the surface reflections. However, the emphasis is slightly different now. In particular, it should be clearly understood that the focusing is the very reason for

the infinite pulses to alternate with the finite ones. If the centre were isolated and the first pulse were infinite, one would never observe a finite pulse because focusing that eliminates infinite pressure would never occur. Alternatively, if the first pulse is finite and the centre is isolated, infinite pressure is never observed. The latter would be the case when, for example, a rigid coaxial core is placed inside the shell (Iakovlev, 2004).

It is particularly clear now that the fact that the response functions completely determine the mathematical solution of the 'acoustic' part of the problem is not a coincidence at all. As we have just seen, they capture the very essence of the physics of the interaction as well. Thus, the theoretical importance of studying response functions for various shell systems should never be underestimated.

We note that every point inside the fluid domain experiences twice as many pressure discontinuities as that on the shell surface. This happens because pressure waves that travel back and forth between the centre and the shell reflect from the latter only once during each 'cycle', but pass twice through any other point. From the mathematical point of view, as $r \to 1$ the discontinuities become closer and closer to each other, and finally, at $r = 1$, each pair of discontinuities of ξ_n^i merges to produce a discontinuity of ψ_n^i, Fig. A.1. Note that $\xi_n^i(r, t) = 0$ for all $t < 1 - r$ since the 'signal' from the shell surface has not yet reached the point (r, θ).

We also mention that even though at $r = 0$ Eqs. (58) and (59) are still applicable, the expression for the internal pressure can be considerably simplified in this case. Indeed, if $r = 0$, $\mathrm{J}_n(r\omega_k^n) = 1$ for $n = 0$ and is zero otherwise. Hence,

$$\xi_0^i(0, t) = 2t + 2\sum_{k=1}^{\infty} \frac{1}{\omega_k^0 \mathrm{J}_n(\omega_k^0)} \sin(\omega_k^0 t), \tag{66}$$

and

$$\xi_n^i(0, t) = 0, \quad t \geqslant 0, \ \ n \geqslant 1. \tag{67}$$

Then, the pressure on the axis of the shell is given by

$$\hat{p}_r^i(0, t) = \int_0^t \ddot{w}_0(\eta) \xi_0^i(0, t - \eta)\, \mathrm{d}\eta, \tag{68}$$

where a double over dot denotes the second derivative of a function.

In order to illustrate just how much more challenging dealing with the 'volume' response functions is, we look at the 'worst case scenario' of large n and small r. In particular, Fig. A.2 shows $\xi_{150}^i(0.02, t)$.

As one can see, the function is very close to zero almost everywhere, except for the very close proximities of the points $t = 1$, 3, and 5 (namely, the intervals $L_r^1 = [1 - r, 1 + r]$, $L_r^2 = [3 - r, 3 + r]$, and $L_r^3 = [5 - r, 5]$). As to the behaviour inside those intervals, close-ups of the 'problem areas' have to be considered (insets 1 and 2) from which it is apparent that $\xi_{150}^i(0.02, t)$ is highly oscillating inside $L_r^1 - L_r^3$. It is of particular importance that even though the period of oscillations is extremely small, the amplitude is not. The frequency of the oscillations increases significantly as t approaches the points of discontinuity $t_0^f = 0.98$ and $t_0^s = 1.02$, and yet another set of close-ups is needed to analyze the behaviour of $\xi_{150}^i(0.02, t)$ in the close proximity of those points, insets 3 and 4.

Quite naturally, this mathematical complexity leads to a variety of numerical challenges, of which we mention two. The first is integration of ξ_n^i. As is apparent from Fig. A.2, essentially different integration steps have to be used within different subintervals of the time domain. It was found that, to ensure an acceptable accuracy of the results, the integration step had to be varied from a relatively large values in low-frequency regions (far away from the points of discontinuity) to 10^{-6} or even smaller in high-frequency regions. We would like to particularly emphasize that if in the proximity of the singular points one uses an integration step which is not sufficiently small, the resulting pressure field will be contaminated with very undesirable numerical noise. The nature of this noise is such that on two-dimensional plots of the pressure field it produces a very regular pattern, and appears as a wave of some sort which is hard to distinguish from 'real' waves. The situation is worsened by the fact that the magnitude of the 'noisy' contributions is comparable with that of some second-order 'real' waves, and so in the presence of this type of noise one is in danger of arriving at the wrong conclusions about the physics of the interaction.

The second challenge we mention here is that the series in (58) and (59) converge slower and slower as one approaches the points of discontinuity, especially at small r and large n. To achieve acceptable accuracy for any t but still ensure bearable computational time, the number of terms considered in the corresponding series had to be t-dependent. It changed from a few thousands in the regions far away from the discontinuities to many tens of thousands in the close proximity of those.

Even though the mentioned computational difficulties appear to be quite a significant obstacle, the good news is that since the response functions do not depend on the properties of the shell or fluids, they have to be computed

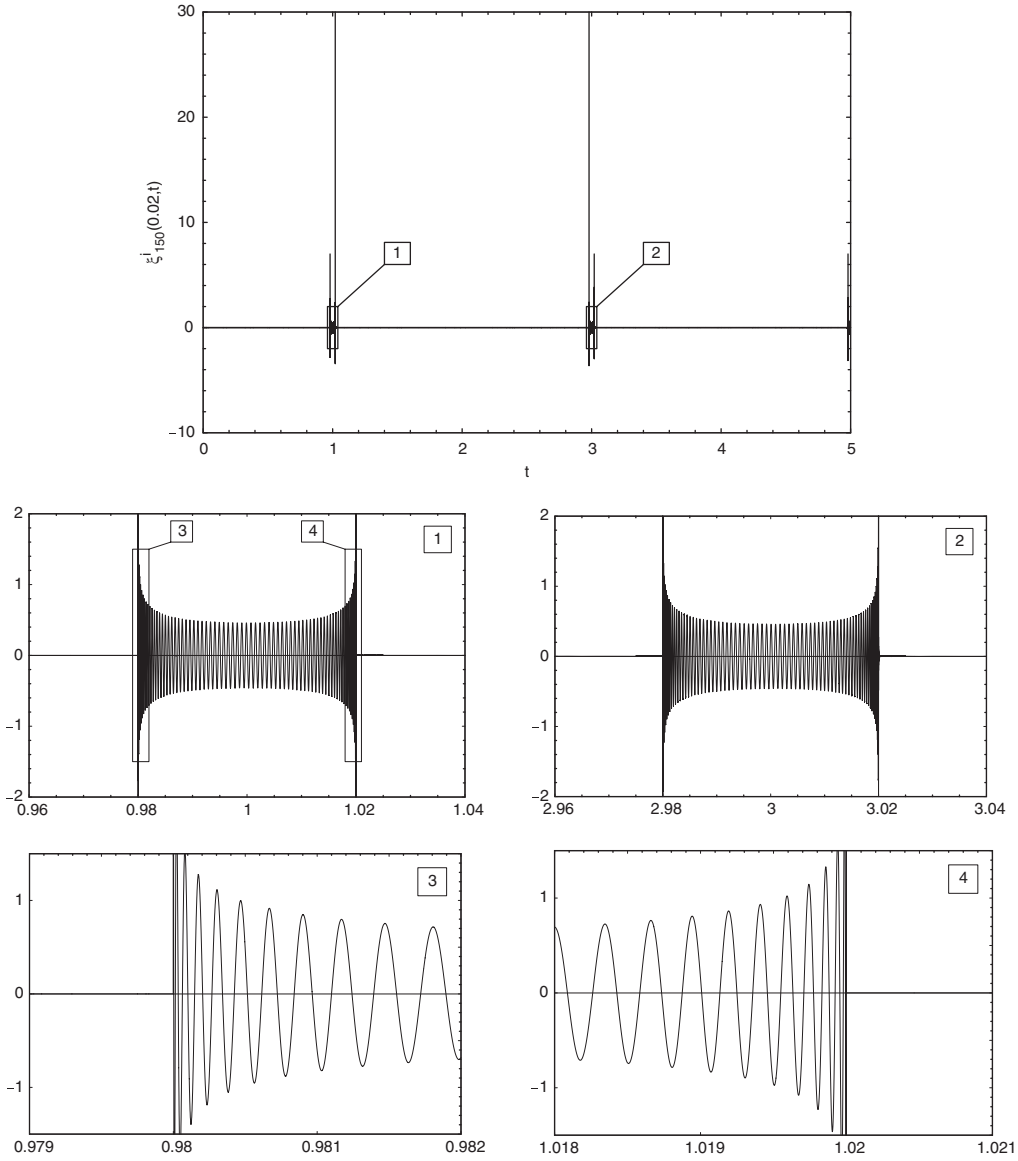

Fig. A.2. Response function $\xi^i_{150}(0.02, t)$.

only once. Because the computations in question have been performed in the present work, future investigations based on the developed model will be much less mathematically challenging and much more time-efficient.

To deal with the numerical challenges inherent to the computation of the 'volume' response functions and their integrals, a software package was developed in C++. Great care was taken to make sure that necessary accuracy was achieved at all t, r, and n. Also, as we emphasized earlier, knowing the dynamics of w along the circumference of the cross-section of the shell is sufficient to simulate the entire internal field. The C++ code was developed with that in mind, i.e. the only input needed to simulate the internal acoustic field is the time-history of w. Such an approach to computation of the acoustic pressure allows one to relatively effortlessly simulate the internal field in any fluid-filled shell for which the normal displacements have been determined either experimentally or numerically.

Appendix B. Incident shock wave

The free-field fluid velocity potential ϕ_0 in a spherical shock wave in the spherical coordinate system centred at the source is governed by the one-dimensional wave equation,

$$\frac{\partial^2\phi_0}{\partial R^2}+\frac{2}{R}\frac{\partial\phi_0}{\partial R}=\frac{1}{c_f^2}\frac{\partial^2\phi_0}{\partial T^2}, \tag{69}$$

where R is the radial coordinate, T is time, and c_f is the sound speed in the fluid. Here it is assumed that $T=0$ corresponds to the moment the shock wave is originated, *not* the moment the shock wave falls on the shell.

The solution of (69) is any function of the form

$$\phi_0=\frac{C}{R}\,G(T-Rc_f^{-1}), \tag{70}$$

where C is an arbitrary constant and G is an arbitrary function of its argument. To model a realistic shock wave propagating in the fluid [e.g., Cole, 1948], i.e. to ensure that ϕ_0 represents a shock wave with exponentially decaying pressure behind the front, we assume

$$G(z)=\mathrm{e}^{-z\lambda^{-1}}\mathrm{H}(z), \tag{71}$$

where λ is the rate of exponential decay and H is the Heaviside step function, $\mathrm{H}(z)=1$ for $z\geqslant 0$, and $\mathrm{H}(z)=0$ otherwise. Substituting (71) into (70), we obtain the potential in such a step-exponential shock wave as

$$\phi_0=\frac{C}{R}\,\mathrm{e}^{-(T-Rc_f^{-1})\lambda^{-1}}\mathrm{H}(T-Rc_f^{-1}), \tag{72}$$

where C is still to be determined. We recall that

$$p_0=-\rho_f\frac{\partial\phi_0}{\partial t}, \tag{73}$$

where p_0 is the incident pressure. Thus, we can write

$$p_0=-\frac{C\rho_f}{R\lambda}\,\mathrm{e}^{-(T-Rc_f^{-1})\lambda^{-1}}\mathrm{H}(T-Rc_f^{-1}). \tag{74}$$

To determine the suitable value of the constant C, we 'calibrate' the incident pressure [e.g., Sprague and Geers (1999)]. Specifically, we choose C such that p_0 is equal to a specific peak value p_α at the moment the shock wave impinges on the shell, i.e. when $R=S_R$ and $T=S_Rc_f^{-1}$, where S_R is the shock wave stand-off, or the distance between the shell and the wave source, $S_R=R_0-r_0$. Then,

$$C=-\frac{\lambda p_\alpha S_R}{\rho_f}. \tag{75}$$

The next step is to express the time T in terms of the 'shell' time τ, where τ is set so that $\tau=0$ corresponds to the instant when the shock wave first contacts the shell, $T=S_Rc_f^{-1}$, and so

$$\tau=T-S_Rc_f^{-1}=T-(R_0-r_0)c_f^{-1}. \tag{76}$$

Finally, we express the radial coordinate R of the source-centred spherical coordinate system in terms of the shell-based cylindrical coordinates (x,ϱ,θ) where x, ϱ, and θ are the axial, radial, and angular coordinates, respectively. It is easy to show that

$$R=\sqrt{R_0^2+x^2+\varrho^2-2R_0\varrho\cos\theta}. \tag{77}$$

We, however, consider a two-dimensional formulation of the problem, i.e. disregard any changes in the axial direction. To satisfy this requirement, we consider the incident pressure in the mid-section of the shell (i.e. $x=0$), and assume that the same pressure profile is applied to the shell for any other x (i.e. we are switching to a 'cylindrical' shock wave with the exponential pressure decay behind the wavefront). Under this assumption, the radial distance R expressed in the polar coordinates (ϱ,θ) based on the axis of the shell is given by

$$R=\sqrt{R_0^2+\varrho^2-2R_0\varrho\cos\theta}. \tag{78}$$

Then, we can write down the expressions for ϕ_0 and p_0 that are used in the actual computations,

$$\phi_0 = -\frac{\lambda p_\alpha S_R}{\rho_f R} \mathrm{e}^{-(\tau - c_f^{-1}(R-S_R))\lambda^{-1}} \mathrm{H}(\tau - c_f^{-1}(R-S_R)) \tag{79}$$

and

$$p_0 = \frac{p_\alpha S_R}{R} \mathrm{e}^{-(\tau - c_f^{-1}(R-S_R))\lambda^{-1}} \mathrm{H}(\tau - c_f^{-1}(R-S_R)). \tag{80}$$

References

van Aanhold, J.E., Meijer, G.J., Lemmen, P.P.M., 1998. Underwater shock response analysis of a floating vessel. Shock and Vibration 5, 53–59.

Abe, A., Ojima, H., Ogawa, T., Babinsky, H., Takayama, K., 1999. Animated display of sequential holographic interferograms of shock wave/vortex propagation. Proceedings of the 22nd International Symposium on Shock Waves, Imperial College, London, UK, pp. 1111–1116.

Ahyi, A.C., Pernod, P., Gatti, O., Latard, V., Merlen, A., Uberall, H., 1998. Experimental demonstration of the pseudo-Rayleigh (A_0) wave. Journal of the Acoustical Society of America 104, 2727–2732.

Andelfinger, U., 1994. Simulations of underwater explosions against submerged structures using the DYSMAS/ELC code—Part A. Proceedings of the 65th Shock and Vibration Symposium, vol. II, San Diego, California, USA, pp. 243–251.

Apazidis, N., 2003. Focusing of strong shocks in an elliptic cavity. Shock Waves 13, 91–101.

Bao, X.L., Raju, P.K., Uberall, H., 1999. Circumferential waves on an immersed, fluid-filled elastic cylindrical shell. Journal of the Acoustical Society of America 105, 2704–2709.

Ben-Dor, G., 1991. Shock Wave Reflection Phenomena. Springer, New York, USA.

Ben-Dor, G., Takayama, K., 1992. The phenomena of shock wave reflection—a review of unsolved problems and future research needs. Shock Waves 2, 211–223.

Bryson, A.E., Gross, R.W.F., 1961. Diffraction of strong shocks by cones, cylinders, and spheres. Journal of Fluid Mechanics 10, 1–16.

Chambers, G., Sandusky, H., Zerilli, F., Rye, K., Tussing, R., Forbes, J., 2001. Pressure measurements on a deforming surface in response to an underwater explosion in a water-filled aluminum tube. Shock and Vibration 8, 1–7.

Cole, R.H., 1948. Underwater Explosions. Dover Publications, New York.

Drikakis, D., Ofengeim, D., Timofeev, E., Voionovich, P., 1997. Computation of non-stationary shock-wave/cylinder interaction using adaptive-grid methods. Journal of Fluids and Structures 11, 665–691.

Eidelman, S., Yang, X., Lottati, I., 1993. Numerical simulation of shock wave reflection and diffraction in a dusty gas. Proceedings of the 19th International Symposium on Shock Waves, Marseille, France, pp. 56–60.

Geers, T.L., 1969. Excitation of an elastic cylindrical shell by a transient acoustic wave. Journal of Applied Mechanics 36, 459–469.

Geers, T.L., 1972. Scattering of a transient acoustic wave by an elastic cylindrical shell. Journal of the Acoustical Society of America 51, 1640–1651.

Geers, T.L., Zhang, P., 1994a. Doubly asymptotic approximations for submerged structures with internal fluid volumes: formulation. Journal of Applied Mechanics 61, 893–899.

Geers, T.L., Zhang, P., 1994b. Doubly asymptotic approximations for submerged structures with internal fluid volumes: evaluation. Journal of Applied Mechanics 61, 900–906.

Glass, I.I., Kaca, J., Zhang, D.L., Glaz, H.M., Bell, J.B., Trangenstein, J.A., Collins, J.P., 1989. Diffraction of planar shock waves over half-diamond and semicircular cylinders: an experimental and numerical comparison. Proceedings of the 17th International Symposium on Shock Waves and Shock Tubes, Bethlehem, Pennsylvania, USA, pp. 246–251.

Haywood, J.H., 1958. Response of an elastic cylindrical shell to a pressure pulse. Quarterly Journal of Mechanics and Applied Mathematics 11, 129–141.

Heilig, G., 1999 Shock-induced flow past cylinders with various radii. Proceedings of the 22nd International Symposium on Shock Waves, Imperial College, London, UK, pp. 1099–1104.

Heilig, W., 1987. The influence of wall- and shock curvature on shock reflection processes. Proceedings of the 16th International Symposium on Shock Tubes and Waves, Aachen, Germany, pp. 543–549.

Heilig, W.H., 1969. Diffraction of a shock wave by a cylinder. Physics of Fluids 12 (Suppl. I), 154–157.

Hermann, D., Weblau, F.P., Adomeit, G., 1987. Measurements of heat transfer and vortex shedding frequency of cylinders in shock tube cross flow. Proceedings of the 16th International Symposium on Shock Tubes and Waves, Aachen, Germany, pp. 822–830.

Huang, H., 1975. Scattering of spherical pressure pulses by a hard cylinder. Journal of the Acoustical Society of America 58, 310–317.

Huang, H., 1979. Transient response of two fluid-coupled cylindrical elastic shells to an incident pressure pulse. Journal of Applied Mechanics 46, 513–518.

Huang, H., Mair, H., 1996. Neoclassical solution of transient interaction of plane acoustic waves with a spherical elastic shell. Shock and Vibration 3, 85–98.

Huang, H., Wang, Y.F., 1970. Transient interaction of spherical acoustic waves and a cylindrical elastic shell. Journal of the Acoustical Society of America 48, 228–235.

Huang, H., Wang, Y.F., 1971. Early-times interaction of spherical acoustic waves and a cylindrical elastic shell. Journal of the Acoustical Society of America 50, 885–891.

Iakovlev, S., 2002a. Interaction of a spherical shock wave and a submerged fluid-filled circular cylindrical shell. Journal of Sound and Vibration 225, 615–633.

Iakovlev, S., 2002b. On the singular behavior of the inverse Laplace transforms of the functions $I_n(s)/(sI'_n(s))$. Canadian Mathematical Bulletin 45, 399–416.

Iakovlev, S., 2004. Influence of a rigid co-axial core on the stress–strain state of a submerged fluid-filled circular cylindrical shell subjected to a shock wave. Journal of Fluids and Structures 19, 957–984.

Izumi, K., Aso, S., Nishida, M., 1994. Experimental and computational studies focusing processes of shock waves reflected from parabolic cylinders. Shock Waves 3, 213–222.

Jialing, L., Hongli, N., 1997. Study on propagation of blast wave over cylinder in a channel bend. Proceedings of the 21st International Symposium on Shock Waves, Great Keppel Island, Australia, pp. 104–107.

Junger, M.C., Feit, D., 1972. Sound, Structures, and Their Interaction. MIT Press, Cambridge, USA.

Latard, V., Merlen, A., Preobazhenski, V., Ahyi, A.C., 1999. Acoustic scattering of impulsive geometrical waves by a glass sphere in water. Applied Physics Letters 74, 1919–1921.

Liang, C.C., Hsu, C.Y., Lai, W.H., 2000. A study of transient responses of a submerged spherical shell under shock waves. Ocean Engineering 28, 71–91.

Liang, S.M., Wu, L.N., Hsu, R.L., 1999. Numerical investigation of axisymmetric shock wave focusing over paraboloid reflectors. Shock Waves 9, 367–379.

Lind, C.A., Cybyk, B.Z., Boris, J.P., 1999. Attenuation of shocks: high Reynolds number porous flows. Proceedings of the 22nd International Symposium on Shock Waves, Imperial College, London, UK, pp. 1135–1140.

Mair, H.U., 1999a. Review: Hydrocodes for structural response to underwater explosions. Shock and Vibration 6, 81–96.

Mair, H.U., 1999b. Benchmarks for submerged structure response to underwater explosion. Shock and Vibration 6, 169–181.

Merlen, A., Pernod, P., Ahyi, A., Kemmou, A., 1995. Shock-wave diffraction by an elastic sphere in water. Proceedings of the 20th International Symposium on Shock Waves, Pasadena, California, USA, vol. I, pp. 513–518.

Mindlin, R.D., Bleich, H.H., 1953. Response of an elastic cylindrical shell to a transverse step shock wave. Journal of Applied Mechanics 20, 189–195.

Neubauer, W.G., Dragonette, L.R., 1970. Observation of waves radiated from circular cylinders caused by an incident pulse. Journal of the Acoustical Society of America 48, 1135–1149.

Oakley, J.G., Puranik, B.P., Anderson, M.H., Peterson, R.R., Bonazza, R., Weaver, R.P., Gittings, M.L., 1999. An investigation of shock-cylinder interaction. Proceedings of the 22nd International Symposium on Shock Waves, Imperial College, London, UK, pp. 941–946.

Oakley, J.G., Anderson, M.H., Wang, S., Bonazza, R., 2001. Shock loading of a cylinder bank with imaging and pressure measurements. Proceedings of the 23nd International Symposium on Shock Waves, Fort Worth, Texas, USA, pp. 589–595.

Ofengeim, D.Kh., Drikakis, D., 1997. Simulation of blast wave propagation over a cylinder. Shock Waves 7, 305–317.

Park, I.-K., Kim, J.-C., An, C.-W., Cho, D.-S., 2003. Measurement of naval ship response to underwater explosion shock loading. Shock and Vibration 10, 365–377.

Peralta, L.A., Raynor, S., 1964. Initial response of a fluid-filled elastic, circular, cylindrical shell to a shock wave in acoustic medium. Journal of the Acoustical Society of America 36, 476–488.

Phan, K.C., Stollery, J.L., 1985. On the effects of shock wave reflection in a confined space. Proceedings of the 15th International Symposium on Shock Waves and Shock Tubes, Berkeley, California, USA, pp. 139–145.

Quentin, G., Talmant, M., 1989. The plane plate model applied to the scattering of the ultrasonic waves from cylindrical shells. Elastic Wave Propagation, Proceedings of the 2nd IUTAM-IUPAP Symposium on Elastic Wave Propagation, Galway, Ireland, pp. 477–482.

Sandusky, H., Chambers, P., Zerilli, F., Fabini, L., Gottwald, W., 1999. Dynamic measurements of plastic deformation in a water-filled aluminum tube in response to detonation of a small explosives charge. Shock and Vibration 6, 125–132.

Schedin, S., Gren, P.O., Wahlin, A., 1997. Shock waves in an elliptical cavity with varying height. Shock Waves 7, 343–350.

Scott, J.F.M., 1988. The free modes of propagation of an infinite fluid-loaded thin cylindrical shell. Journal of Sound and Vibration 125, 241–280.

Sessarego, J.-P., Sageloli, J., Gazanhes, C., 1997. Two Scholte–Stoneley waves on doubly fluid-loaded plates and shells. Journal of the Acoustical Society of America 101, 135–142.

Shin, Y., Santiago, L.D., 1998. Surface ship shock modelling and simulation: two-dimensional analysis. Shock and Vibration 5, 129–137.

Sommerfeld, M., Muller, H.M., 1988. Experimental and numerical studies of shock wave focusing in water. Experiments in Fluids 6, 209–216.

Sprague, M.A., Geers, T.L., 1999. Response of empty and fluid-filled, submerged spherical shells to plane and spherical, step-exponential acoustic waves. Shock and Vibration 6, 147–157.

Sturtevant, B., Kulkarny, V.A., 1976. The focusing of weak shock waves. Journal of Fluid Mechanics 73, 651–671.

Sugiyama, H., Arai, T., Nagumo, H., Sueki, H., Izumi, M., Takayama, K., 1989. An experimental and numerical study of the shock wave-induced flows past a circular cylinder in a dusty-gas shock tube. Proceedings of the 17th International Symposium on Shock Waves and Shock Tubes, Bethlehem, Pennsylvania, USA, pp. 258–263.

Sun, M., 1998. Numerical and experimental studies of shock wave interaction with bodies. Ph.D. Thesis, Tohoku University, Japan.

Sun, M., 2004. Personal communication. Institute of Fluid Science, Tohoku University, Sendai, Japan.

Sun, M., Takayama, K., 1996. A holographic interferometric study of shock wave focusing in a circular reflector. Shock Waves 6, 323–336.

Sun, M., Takayama, K., 1999. Conservative smoothing on an adaptive quadrilateral grid. Journal of Computational Physics 150, 143–180.

Sun, M., Yada, K., Jagadeesh, G., Odonera, O., Ogawa, T., Takayama, K., 2003. A study of shock wave interaction with a rotating cylinder. Shock Waves 12, 479–485.

Takano, Y., Hayashi, K., and Goto, T., 1997. A computational procedure for interactions of shock waves with solid materials in liquid. Proceedings of the 21st International Symposium on Shock Waves, Great Keppel Island, Australia, pp. 1039–1044.

Takayama, K., 1987. Holographic interferometric study of shock wave propagation in two-phase media. Proceedings of the 16th International Symposium on Shock Tubes and Waves, Aachen, Germany, pp. 52–62.

Takayama, K., 1993. Optical flow visualization of shock wave phenomena (Paul Vieille Memorial Lecture). Proceedings of the 19th International Symposium on Shock Waves, Marseille, France, pp. 8–16.

Ugural, A.C., 1981. Stresses in Plates and Shells. McGraw-Hill Book Company, New York.

Wardlaw Jr., A.B., Luton, J.A., 2000. Fluid–structure interaction mechanisms for close-in explosions. Shock and Vibration 7, 265–275.

Yang, J.Y., Liu, Y., 1987. Computation of shock wave reflection by circular cylinders. AIAA Journal 25, 683–689.

Yang, J.Y., Lombard, C.K., Bershader, D., 1985. Computation of nonstationary shock wave diffraction from curved surfaces. Proceedings of the 15th International Symposium on Shock Waves and Shock Tubes, Berkeley, California, USA, pp. 399–405.

Yang, J.Y., Hsu, C.A., Jiang, C.T., Muller, B., 1991. Computation of shock diffraction in external and internal flows. Proceedings of the 18th International Symposium on Shock Waves, Sendai, Japan, pp. 1063–1068.